

Mechanics of Multicentrosomal Clustering in Bipolar Mitotic Spindles

Saptarshi Chatterjee,¹ Apurba Sarkar,¹ Jie Zhu,² Alexei Khodjakov,^{3,4} Alex Mogilner,^{5,*} and Raja Paul^{1,*}

¹Indian Association for the Cultivation of Science, Kolkata, India; ²Gerber Technology, Tolland, Connecticut; ³Wadsworth Center, New York State Department of Health, Albany, New York; ⁴Rensselaer Polytechnic Institute, Troy, New York; and ⁵Courant Institute and Department of Biology, New York University, New York, New York

ABSTRACT To segregate chromosomes in mitosis, cells assemble a mitotic spindle, a molecular machine with centrosomes at two opposing cell poles and chromosomes at the equator. Microtubules and molecular motors connect the poles to kinetochores, specialized protein assemblies on the centromere regions of the chromosomes. Bipolarity of the spindle is crucial for the proper cell division, and two centrosomes in animal cells naturally become two spindle poles. Cancer cells are often multicentrosomal, yet they are able to assemble bipolar spindles by clustering centrosomes into two spindle poles. Mechanisms of this clustering are debated. In this study, we computationally screen effective forces between 1) centrosomes, 2) centrosomes and kinetochores, 3) centrosomes and chromosome arms, and 4) centrosomes and cell cortex to understand mechanics that determines three-dimensional spindle architecture. To do this, we use the stochastic Monte Carlo search for stable mechanical equilibria in the effective energy landscape of the spindle. We find that the following conditions have to be met to robustly assemble the bipolar spindle in a multicentrosomal cell: 1) the strengths of centrosomes' attraction to each other and to the cell cortex have to be proportional to each other and 2) the strengths of centrosomes' attraction to kinetochores and repulsion from the chromosome arms have to be proportional to each other. We also find that three other spindle configurations emerge if these conditions are not met: 1) collapsed, 2) monopolar, and 3) multipolar spindles, and the computational screen reveals mechanical conditions for these abnormal spindles.

SIGNIFICANCE To segregate chromosomes, cells assemble a bipolar mitotic spindle. Multiple mechanical forces generated by microtubules and molecular motors in the spindle govern the spindle architecture, but it is unclear what force balances support the bipolarity of the spindle. This problem is especially difficult and important in cancer cells, which often have multiple centrosomes that somehow are able to cluster into two spindle poles. By using stochastic energy minimization in an effective energy landscape of the spindle and computationally screening forces, we find mechanical conditions for mono-, multi-, and bipolar spindles. We predict how microtubule and motor parameters have to be regulated in mitosis in multicentrosomal cells.

INTRODUCTION

Many cell biological problems converge on understanding the dynamic architecture of molecular machines (1), for example, mitotic spindles. During cell division, cells assemble the spindle to segregate chromosomes (2). It is crucial that the spindle is bipolar (Fig. 1) so that sister chromatids segregate to two opposite poles and end in two daughter cells. In animal cells, centrosomes (CSs)

are organelles nucleating and anchoring minus ends of microtubules (MTs); a dynamic MT network spans the space between CSs and chromosomes and connects to chromosomes by plus ends. Thus, despite the fact that the exact role of CSs in the process of spindle assembly is not simple and varies between different cell types (3), more often than not, CSs organize the spindle poles (4). It is, therefore, not surprising that having exactly two CSs per mitotic cell is fundamentally related to the bipolarity of the spindle.

Normally, CSs duplicate once per cell cycle, but various perturbations can result in the accumulation of more than two CSs per cell (5,6). Multi-CS cells are a common feature of tumors, but certain healthy cells in our body

Submitted December 17, 2019, and accepted for publication June 4, 2020.

*Correspondence: mogilner@cims.nyu.edu or raja.paul@iacs.res.in

Saptarshi Chatterjee and Apurba Sarkar contributed equally to this work.

Editor: Dimitrios Vavylonis.

<https://doi.org/10.1016/j.bpj.2020.06.004>

© 2020 Biophysical Society.

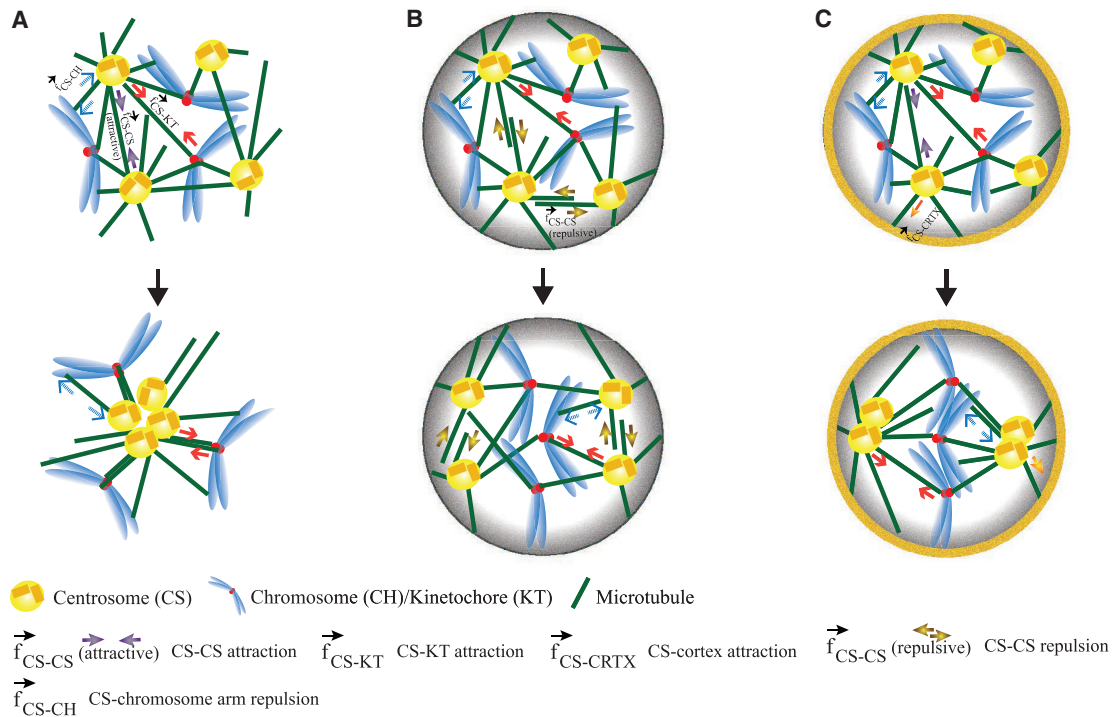


FIGURE 1 Model schematics depicting the individual forces governing the mechanics of multicentrosomal spindles. (A) CSs aggregate into a single cluster, and a monopolar spindle emerges when CSs attract each other (f_{CS-CS}) or KTs (f_{CS-KT}) and repel chromosome arms (f_{CS-CH}). (B) In confinement of the cell volume but without active interaction with the cortex, a multipolar spindle emerges when CSs repel each other. (C) CSs aggregate into two clusters at the opposite cell poles, whereas chromosomes gather at the equator, creating a bipolar spindle when CSs are mutually attractive and also are attracted to the cell cortex ($f_{CS-CRTX}$). The orange annular ring denotes the presence of cortical pull. To see this figure in color, go online.

also contain extra CSs, either transiently or permanently (7). The presence of more than two CSs at the onset of mitosis has long been associated with multipolar spindle formation (Fig. 1; (4)). Multiple CSs and multipolar spindles are often correlated with chromosome instability (6,8), aneuploidy (9), erroneous merotelic attachments of chromosomes (10,11), and other defects of chromosome segregation (12).

In recent years, several studies have shown that a process of “CS clustering”—gathering multiple CSs into two groups at the opposing spindle poles—is one of the main pathways leading to the formation of the bipolar spindles in multi-CS cells (4,5). However, not all cells appear to have equal capacity to cluster multiple CSs (11,13); thus, understanding the CS clustering mechanisms is of great importance.

Distinct, but not mutually exclusive, mechanisms for spindle self-organization have been proposed. These mechanisms range from intrinsic chemical and physical, to extrinsic models (14), but the majority of the models are mechanical, relying on a balance of forces as the greatest contributor to the spindle architecture (4,14,15). Chemical and genetic inhibition, molecular screening, and micromanipulation experiments established that a great variety of molecular and geometric factors (reviewed in (4)), including minus-end molecular motors dynein (13) and kinesin-14

(5,12), as well as cell shapes and forces from neighboring cells (5,16,17), act in the CS clustering mechanism.

The role of dynein and kinesin-14 led to two intuitive, but again not mutually exclusive, hypotheses: 1) minus-end molecular motors pull on MTs spanning the distance between two CSs, generating effective inter-CS attraction (Fig. 1; (5)). This attraction force clusters multiple CSs. 2) Dynein concentrated on a patch of the cell cortex and/or cortex contractions can reel in MTs from a few CSs, bringing them together (Fig. 1; (5)). However, a natural question is why do the CSs cluster into exactly two groups? Why do such mechanisms not lead to all CSs clustering into a single group, causing the formation of a monopolar spindle (Fig. 1)? Are these mechanisms, in fact, sufficient to prevent the formation of the multipolar spindles? Are both inter-CS and CS-cortex interactions necessary? All these spindle types—monopolar (18–20), bipolar, and multipolar—have been observed (5,11,12,21), so what are the necessary and sufficient mechanics for the emergence of the bipolar spindle?

Measuring and quantitatively manipulating forces in the spindle is a great challenge (22,23), and so modeling has long been a valuable tool complementing experimental research of all stages and aspects of spindle dynamics (17,24–32). Specifically, force-balance models have been applied to reproduce the observed spindle structures,

both in one-dimensional (19,33,34) and in two-dimensional geometry (19,35). In this study, we introduce a force-balance model in realistic three-dimensional (3D) cell geometry and computationally screen CS-CS, CS-cortex, and CS-chromosome forces to answer the questions posed above.

The most straightforward approach would be agent-based modeling (25,27,31,32), in which all MTs, motors, and organelles are simulated as agents obeying laws of mechanics. Despite the significant advantages of such modeling, it has two drawbacks. First, the possible number of molecular motors' combinations in various parts of the spindle is too great (reviewed in (15)), and the exact mechanics of the collective motor force generation is still far from clear. Second, simulating an agent-based model in three dimensions is so time-consuming that screening many forces and parameters is out of question (36). Therefore, we resort to the "interacting particles" model, in which each CS and chromosome is a particle interacting with other particles by pairwise isotropic forces that depend on the distance between the interacting particles (37). Each such force results from averaged action of stochastic MTs' and motors' dynamics. Furthermore, rather than solving equations of motion of all particles, in this study, we use an energy-minimization approach to determine spindle architectures corresponding to mechanical equilibria (38) in the presence of the combined forces. This approach allows us to rapidly screen the forces and delineates conditions for the emergence of bipolar spindles in multi-CS cells.

We find that these conditions are 1) the strengths of CSs' attraction to each other and the cell cortex have to be proportional to each other; 2) the strengths of CSs' attraction to kinetochores (KTs) and repulsion from the chromosome arms have to be proportional to each other; and 3) CS attraction to the cortex has to be short-ranged, whereas CS interactions with the chromosomes have to be on the scale of the cell size. We also find that three other spindle configurations emerge if these conditions are not met—1) collapsed, 2) monopolar, and 3) multipolar spindles (Fig. 1)—and the computational screen reveals mechanical conditions for these abnormal spindles. The model correctly reproduces the "doughnut-like" distribution of the chromosomes in the spindle and highlights the importance of the initial conditions for the spindle development.

METHODS

There are two types of interacting particles in the model, CSs and chromosomes; in addition, the CSs interact with the cell cortex in a nontrivial way, and chromosomes cannot penetrate the cortex. The CSs and chromosomes reside in the cell, which is a prolate ellipsoid, and the cortex is the two-dimensional surface or boundary of the cell. The particles interact with four types of forces depicted in Fig. 1. Each force is a so-called "conservative" force, and so a potential energy corresponds to each pairwise interaction. The sum of all these pairwise energies constitutes the total potential energy of the system.

Interactions between pairs of CSs

Each CS is a center of an MT aster with MTs undergoing the dynamic instability (39,40). When an MT growing from one CS reaches another CS or overlaps with an MT growing from that other CS, an effectively attractive or repulsive (depending on the motor types) force, f_{CS-CS} , can be generated by molecular motors interacting with these CSs and MTs (Fig. 1). Using conventional assumptions of a large number of isotropically distributed MTs (19,41–43), we introduce the expressions for f_{CS-CS} and for respective potential energy of moving one CS from distance r_1 to r_2 away from another CS:

$$f_{CS-CS} = f_{CS-CS}^{(0)} e^{-r/L_1}, \quad \Delta E_{CS-CS} = -f_{CS-CS}^{(0)} \int_{r_1}^{r_2} e^{-r/L_1} dr. \quad (1)$$

Here, $f_{CS-CS}^{(0)}$ is the force between a pair of proximal CSs, r is the distance between CSs, and L_1 is the spatial range of the force. Here, we utilize one of the simplest and most frequently used exponentially decreasing spatial dependence of the force; in the Supporting Materials and Methods, we explore other spatial dependencies.

Interaction between a CS and a KT

There are two interactions between the CSs and chromosomes: CS-KT interactions and interactions of CSs with chromosome arms. The so-called K-fibers—MT bundles—connect the CS-KT pairs, and molecular motors on the KT and K-fibers generate net CS-KT attraction force (Fig. 1; (44)). We use the simplest assumption that this force is constant and length independent (19,45): $f_{CS-KT} = f_{CS-KT}^{(0)}$. In certain cases, for example, when we simulate the CSs and chromosomes not restricted by the cell boundary, we use a cutoff distance for the CS-KT force such that the force is constant below the cutoff and equal to zero above the cutoff. The corresponding potential energy is

$$\Delta E_{CS-KT} = -f_{CS-KT}^{(0)} \int_{r_1}^{r_2} dr. \quad (2)$$

Interaction between a CS and a chromosome arm

Another interaction is a repulsion between a CS and chromosome arms, f_{CS-CH} (Fig. 1). This force originates both from MT polymerization forces and from kinesins on the arms interacting with the MT plus ends, and it decreases with distance (46–50). We use the following expression for this force and respective potential energy:

$$f_{CS-CH} = f_{CS-CH}^{(0)} e^{-r/L_1}, \quad \Delta E_{CS-CH} = -f_{CS-CH}^{(0)} \int_{r_1}^{r_2} e^{-r/L_1} dr. \quad (3)$$

Note that all three pairwise forces introduced above are between point-like particles, and they are directed along the vectors connecting respective pairs of bodies. CS-KT and CS-chromosome arm forces between a given CS and a given chromosome are directed along the same line, as KT and chromosome arms of a given chromosome are the same point-like particle in the model. In a way, we exploit the fact that in one chromosome, the centers of mass of both KT and chromosome arms are close together, in the small vicinity of the centromeric region. Thus, for a single chromosome, we use one force vector between the CS and KT and another, parallel force vector between the CS and respective chromosome arms instead of the spatially distributed force densities. There is still a difference between the KT and

respective chromosome arms, in the sense that respective forces, though parallel, may have different amplitudes and distance (to CS) dependence. For example, the size of the chromosome arms may affect the magnitude of the CS-CH repulsion force. Note also that the CS-CS and CS-chromosome arm forces are assumed to have the same ranges; the underlying assumption is that average lengths of MTs connecting the CSs and extending from the CSs to the chromosome arms are the same.

Interaction between a CS and the cortex

MTs from the CSs reach the cortex on the inner cell boundary, and dynein motors on the cortex pull on these MTs, generating the attraction (51–53). We use the following expression for this force:

$$\mathbf{f}_{CS-CRTX}(\mathbf{r}) = f_{CS-CRTX}^{(0)} \int_{\Omega} e^{-|\mathbf{r}-\mathbf{y}|/L_2} \frac{(\mathbf{y}-\mathbf{r})}{|\mathbf{r}-\mathbf{y}|} d\mathbf{y}. \quad (4)$$

Here, L_2 is the average range of the attraction to the cortex, \mathbf{y} is the coordinate of a point on the cell surface, and \mathbf{r} is the 3D coordinate of the CS. The integration is over the cell surface Ω ; in the simulations, the surface is approximated by a discrete grid, as explained below, and the integral becomes the sum over the grid's nodes. The corresponding energy of moving the CS from point \mathbf{r}_1 to point \mathbf{r}_2 is

$$\Delta E_{CS-CRTX}(\mathbf{r}_1, \mathbf{r}_2) = - \int_C \mathbf{f}_{CS-CRTX}(\mathbf{r}) \cdot d\mathbf{r}, \quad (5)$$

where C is a segment starting at \mathbf{r}_1 and ending at \mathbf{r}_2 .

Numerical implementation and energy minimization

In principle, we could have solved equations of motion for the CSs and chromosomes as follows: $z_i d\mathbf{r}_i/dt = \mathbf{G}(\mathbf{r}_i) + \sum \mathbf{F}(\mathbf{r}_i - \mathbf{r}_j)$, where z_i is the drag coefficient, \mathbf{r}_i is the position of the i^{th} particle, \mathbf{r}_j are positions of all other particles, $\mathbf{F}(\cdot)$ are the pairwise forces, and $\mathbf{G}(\cdot)$ is the force from the cortex. However, the rules of movement are in fact unknown, and in any case, we are only interested in the mechanical equilibria. Thus, we introduce the total system's mechanical energy: $E = P_1(\mathbf{r}_i) + \sum P_2(\mathbf{r}_i - \mathbf{r}_j)$, where P_1 and P_2 are the potential energies corresponding to the cortex and other forces introduced above, and search for the geometric configurations minimizing this energy. Such an approach was considered and justified in applications to macroscopic biological problems (54,55). Considering cell states as minima in the energy landscapes is gaining popularity (56); note that we consider a well-defined mechanical energy, as in (55), rather than less concrete total energy, which is not easy to define for a cell. Note also that computer simulations are necessary to explore the model energy landscapes because mechanical equilibria of models even simpler than ours can be very complex (57).

In most of the simulations, we consider eight CSs and 46 chromosomes, which are represented by point-like particles. There is a steric repulsion between pairs of chromosomes that scales as inverse square mutual distance and is on when the mutual distance falls below two units of the numerical grid. The steric repulsion between two CSs or between CSs and chromosomes is not considered explicitly, but one particle is prohibited from moving onto a site, which is already occupied by any other particle. The results do not depend sensitively on the steric repulsion range (Fig. S7 C). When the spindle is simulated within the cell, CSs and chromosomes are not allowed to pass through the cell boundary.

In simulations without the cell, we chose a large cubic lattice of size $120 \times 120 \times 120 \mu\text{m}^3$, and all the CSs and chromosomes were distributed randomly within a small sphere at the center of this lattice at the onset of the

simulation. In the cellular geometry, a prolate ellipsoid with semiaxes 20, 15, and $15 \mu\text{m}$ is introduced, and the chromosomes and CSs are initially randomly placed within the confinement. The cell volume is fragmented into a 3D cubic lattice grid. The grid size is $1 \mu\text{m}$ for all cases. The ellipsoid of the cortex is discretized into a finite number of approximately equidistant nodes with the grid size similar to that in the cell volume.

The configuration of the system is updated using the Monte Carlo method in the following manner:

- 1) A CS or a chromosome is selected randomly.
- 2) If it is a CS, move it to a vacant neighboring site chosen randomly and calculate the respective energy change ΔE for moving it from initial position r_1 (node from which the CS moved) to a neighboring position r_2 (node to which the CS moved) by adding ΔE_{CS-CS} , ΔE_{CS-CH} , ΔE_{CS-KT} and $\Delta E_{CS-CRTX}$ (the latter, if the spindle is in the cell).
- 3) If it is a chromosome, do the same, but the energy change is calculated by adding ΔE_{CS-CH} and ΔE_{CS-KT} only.
- 4) The move is accepted if $\Delta E \leq 0$, or else the move is accepted with the probability $p = e^{-\beta \Delta E}$ (Boltzmann weight), where β is the inverse of an effective thermal energy (temperature) required to update the configuration (58). Effective temperature, $1/\beta$, was chosen from numerical trials. As we report in the [Supporting Materials and Methods](#), the energy differences and the energy barriers between local minima in the spindle energy landscape are on the order of $100 \text{ pN} \times \mu\text{m}$. When the chosen temperature is much lower than this characteristic value, the spindle in the simulations is frozen in a minimum near an initial configuration and does not evolve. When the chosen temperature is much higher, the spindle never settles in any energy minimum and keeps jumping randomly between configurations. Thus, we used $\beta = 100 \text{ pN} \times \mu\text{m}$, which is on the order of the energy barriers between local minima in the spindle energy landscape. A fewfold changes in temperature do not change the results significantly (Fig. S7 D).
- 5) The simulations are carried out until a stable equilibrium configuration is achieved. More precisely, we calculate the energies of the system during 1000 time steps, by the end of which the system is normally not evolving and energy is not changing. Then, we repeat the same procedure for the next 1000 time steps as well. If the energy difference between the earlier average at the end of the first run and the latter average is less than a threshold of ($\sim \pm 1 \text{ pN} \times \mu\text{m}$), we conclude that the system has attained equilibrium. The equilibrium statistics have been obtained by averaging over ~ 100 – 200 random initial configurations. In the equilibrium configuration, if two or more CSs are within a distance L_{merge} (which is equal to $1.5 \mu\text{m}$, corresponding to when two CSs are in the neighboring nodes of the numerical grid), they are considered to be clustered.

The model parameters are listed in [Table S1](#). The code for the Monte Carlo simulation written in C can be downloaded from the [Supporting Materials and Methods](#). The data analysis and plotting have been carried out in MATLAB (The MathWorks, Natick, MA). A single simulation run takes ~ 40 min of real time until a mechanical equilibrium is achieved (in Intel(R) Xeon(R) CPU having clock speed 2.20 GHz, RAM 50 GB).

RESULTS

We simulated the model with various combinations of the four principal forces; detailed results are reported below and depicted in [Figs. 2, 3, and 4](#). In brief, first, we simulated the spindle in the absence of the cell boundary, essentially considering the spindle in an unconfined space. Bipolar spindles do emerge in these simulations, but not robustly (Fig. 2). Then, we introduced the cell boundary and cortex and simulated either noninteracting or mutually repulsive CSs and again did not detect the robust bipolarity (Fig. 3).

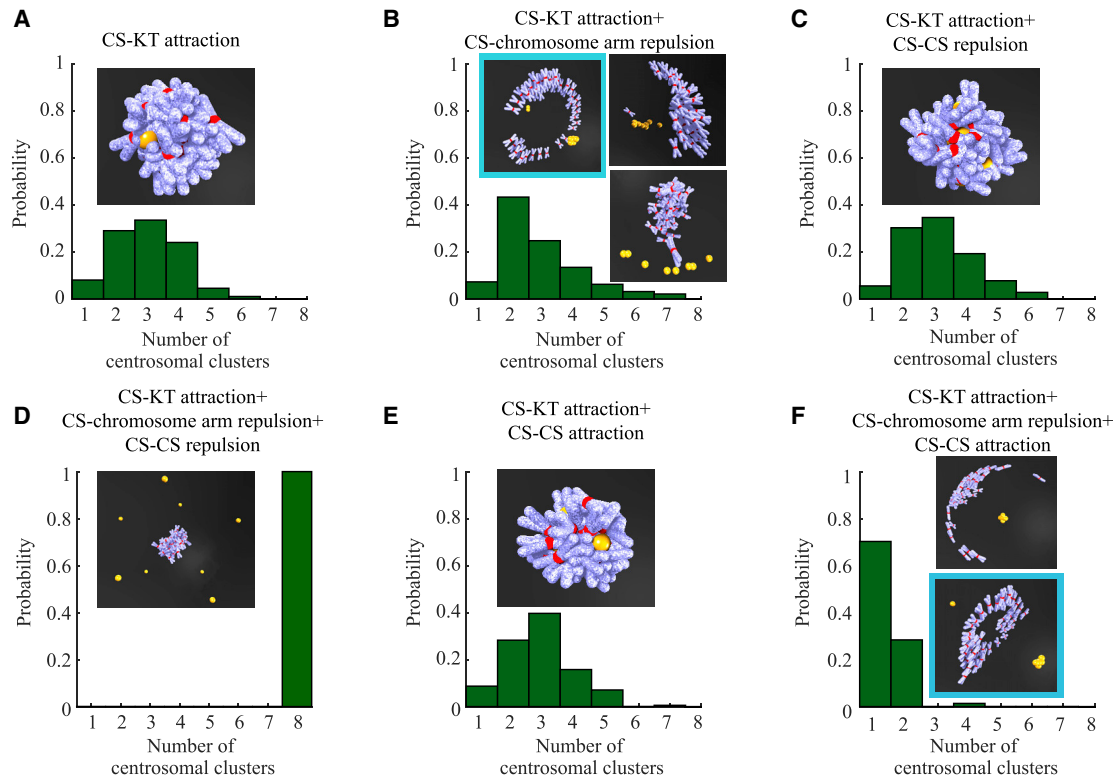


FIGURE 2 Spindle assembly in an unconfined geometry. CSs are yellow; chromosome arms are blue and white; KTs are red. Representative simulation snapshots for bipolar configurations are shown in the inset in a cyan frame. (A) The spindle collapses—both CSs and chromosomes aggregate—in the sole presence of CS-KT attraction. (B) Both bipolar and multipolar with a small number of monopolar spindles develop when the CS-KT attraction is combined with the CS-chromosome arm repulsion. (C) The CS-CS repulsion does not rescue the spindle from the collapse in the presence of the CS-KT attraction and absence of the CS-chromosome arm repulsion. (D) Multipolar spindles emerge in presence of CS-CS repulsion when the CS-KT attraction is combined with the CS-chromosome arm repulsion. (E) The spindle collapses when CS-KT attraction is supplemented with the CS-CS attraction. (F) Monopolar and bipolar spindles emerge in the presence of the CS-CS attraction, CS-KT attraction, and CS-chromosome arm repulsion. To see this figure in color, go online.

We found that the bipolar spindle emerges robustly when the CSs are attracted to each other and the cortex and interact with both KTs and chromosome arms (Fig. 4). In the end, we explore the dependence of the spindle architecture on mechanical, geometric, and structural parameters and initial conditions (Fig. 5). Note that in the figures and videos, the chromosome arms shown in the computational figures are there for the visual effect only because in the models, the chromosomes are point-like. The statistics of the simulated spindles is summarized in Table S2.

Bipolar spindles do not assemble robustly in unconfined geometry

We first explored the emerging spindle architecture without the complexity of interacting with the cortex or being restricted by the cell geometry. If only one type of force, the CS-KT attraction, is present, the spindle collapses (Fig. 2 A, inset): all CSs and chromosomes aggregate together. This result is easy to understand: attraction brings the chromosomes to the CSs, whereas this very same attraction brings other CSs to the aggregate. Note that the emerging number

of the CS clusters varies (Fig. 2), depending on the initial conditions. All these clusters are very close to each other; they do not merge because of the steric repulsion (volume exclusion) effect; the effective energy barrier of pushing crowded chromosomes between CSs out of the way is too high.

Adding the CS-chromosome arm repulsion to the CS-KT attraction rescues the spindle: $\sim 40\%$ of the emerged spindles are bipolar (Fig. 2 B). The repulsion prevents the CSs and the chromosomes from collapsing onto each other. Indeed, because the CS-KT force is attractive and distance independent, whereas the CS-chromosomal arm force is repulsive, decreases with distance, and is greater than CS-KT attraction at small distances, there is a stable mechanical equilibrium such that the CSs and chromosomes tend to rest at a finite distance from each other. Note that in the emerged bipolar spindle at the inset of Fig. 2 B, the chromosomes gather into a “doughnut,” and CSs are in two clusters equidistant from the chromosomes. However, the bipolar geometry is not robust: many multipolar or monopolar spindles emerge, with chromosomes aggregating into one complex-shaped manifold, and CSs are again equidistant from this manifold, but not biclustered (Fig. 2 B, inset).

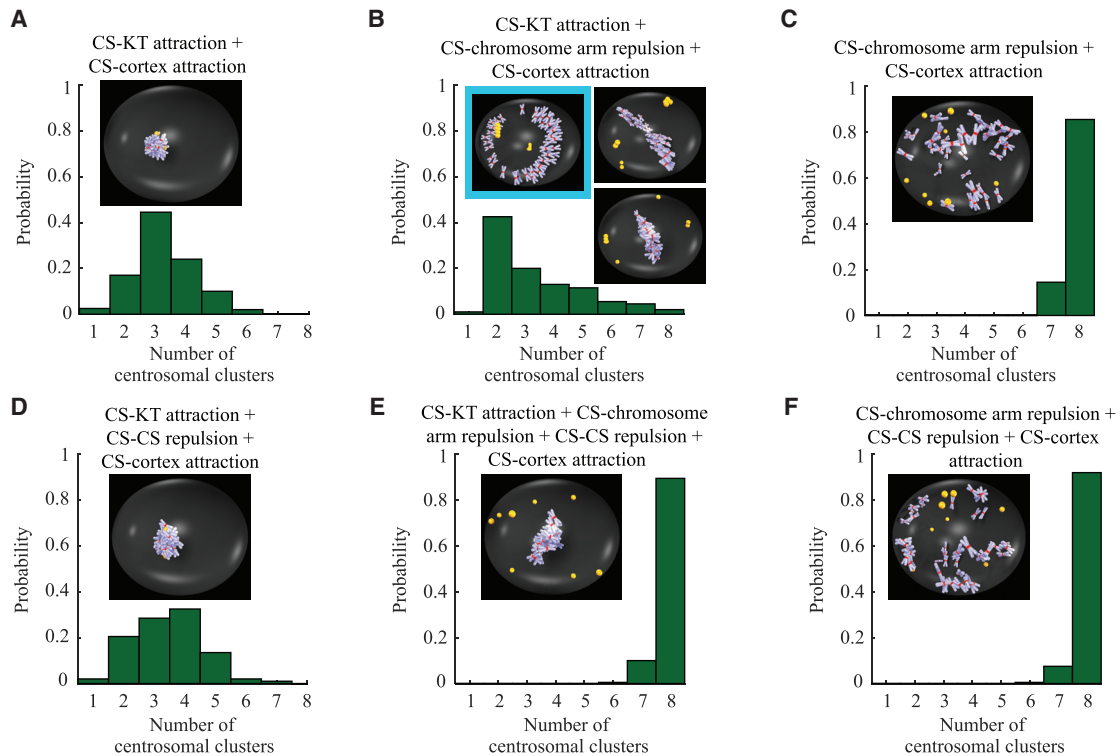


FIGURE 3 Spindle assembly in the presence of the CS-cortex attraction without CS-CS attraction. CSs are yellow; chromosome arms are blue and white; KTs are red. Representative simulation snapshots for bipolar configurations in the inset in cyan frame. (A) A collapsed spindle in the presence of the CS-KT attraction and the absence of the inter-CS interaction. (B) Nonrobust emergence of the bipolar spindle in the presence of the CS-KT attraction and CS-chromosome arm repulsion and in the absence of the inter-CS interaction. (C) Multipolar spindles develop under the sole influence of CS-chromosome arm repulsion. (D) A collapsed spindle when the CS-KT attraction is supplemented by the inter-CS repulsion. (E) Multipolar spindles develop when the CS-KT attraction and CS-chromosome arm repulsion are supplemented by the inter-CS repulsion. (F) Multipolar spindles develop when the CS-chromosome arm repulsion is combined with inter-CS repulsion. To see this figure in color, go online.

If, instead of the CS-chromosome arm repulsion, only CS-CS repulsion is combined with the CS-KT attraction, the collapsed spindles are not rescued (Fig. 2 C). The reason is that the total energies of both CS-KT attraction and CS-chromosome arm repulsion scale as the product of the numbers of the CSs and chromosomes, whereas the energy of the CS-CS interactions scales with the square of the CS number. The number of CSs is much smaller (more than fivefold) than the number of the chromosomes, and the energy of attraction, in this case, overwhelms the repulsive energy.

If we add the CS-CS repulsion to the interactions of the CSs, KTs, and chromosome arms in the case depicted in Fig. 2 B, the CSs tend to stay at a constant equilibrium distance from the chromosomes, and also as far as possible from each other. This leads to the multipolar spindles, in which all chromosomes aggregate at the center, whereas the CSs are scattered uniformly across a spherical surface centered at the chromosomal crowd (Fig. 2 D).

Finally, we turned to the case when CSs are mutually attractive. As expected, when only attractive interactions—CSs attract each other and KTs—are present, the spindle collapses (Fig. 2 E).

When we add the CS-CS attraction to the case of Fig. 2 B—combined CS-KT attraction and CS-chromosome arm repulsion—the multipolar spindles disappear because now the CSs attract each other, and the majority of the spindles are monopolar, with a single CS cluster at the center and chromosomes scattered at a spherical surface centered at the CS cluster (Fig. 2 F; Video S1). However, some bipolar spindles also emerge, with the architecture similar to those in the absence of the CS-CS attraction. The reason is that the chromosomal “doughnut” in the middle repels the CS clusters at both sides away from the middle, creating the energy barriers, which the CS-CS attraction cannot overcome.

In Fig. 2, A, C, and E, we obtain a majority of collapsed spindles, whereas in Fig. 2 F, we get a majority of monopolar clusters. The collapsed spindle, in our classification, is the one in which both CSs and chromosomes are aggregated into a tight cluster (rigorously speaking, all bodies in the cell belong to one interconnected cluster if two bodies are considered connected when the distance between them is no more than $2 \mu\text{m}$). The monopolar spindle, on the other hand, is the one with CSs being aggregated into a tight cluster, whereas chromosomes are positioned away from the CS

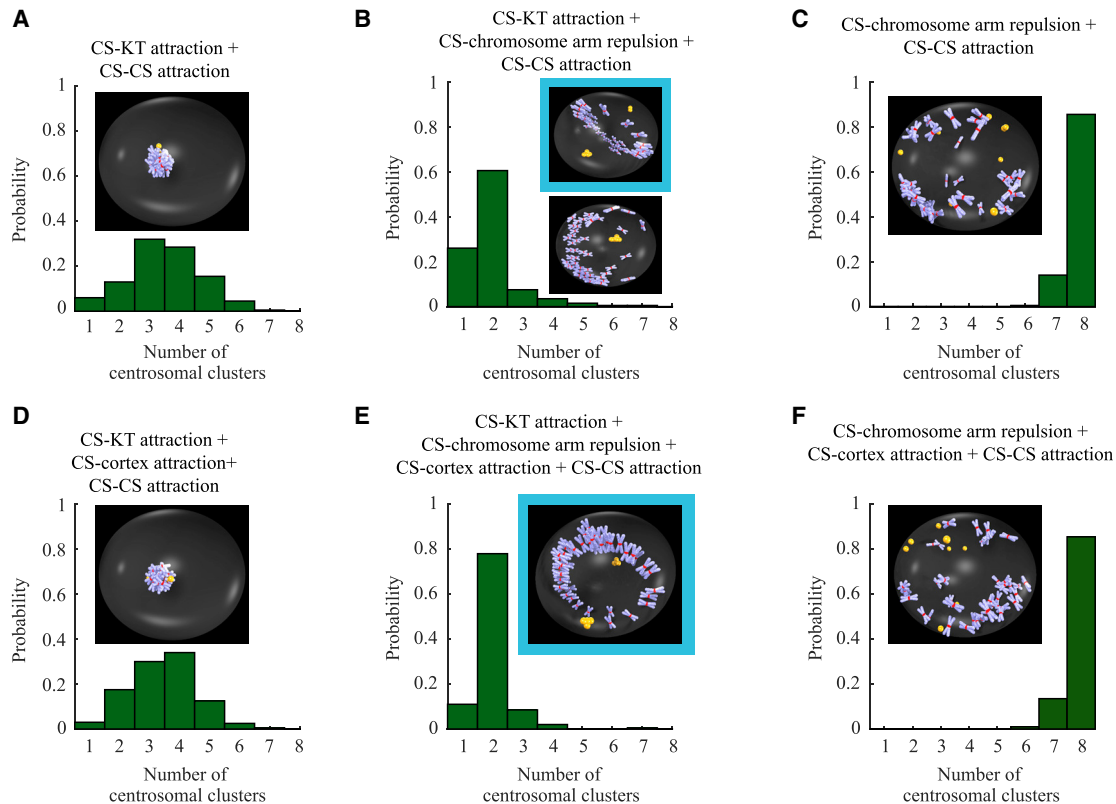


FIGURE 4 Spindle assembly in the presence of the CS attraction to each other and to the cortex. In all simulations reported here, the CS-CS attraction is present. CSs are yellow; chromosome arms are blue and white; KTs are red. Representative simulation snapshots for bipolar configurations in the inset in cyan frame. (A) Spindles collapse when CSs are attracted to KTs without the CS-cortex attraction. (B) Bipolar spindles emerge more robustly with the combination of the CS-KT attraction and CS-chromosome arm repulsion in the absence of the CS-cortex attraction. (C) Multipolar spindles develop when only the CS-chromosome arm repulsion, but not CS-KT attraction, acts in the absence of the CS-cortex attraction. (D) Spindles collapse when CSs are attracted to KTs and to the cortex. (E) Bipolar spindles evolve most robustly when the CS-cortex attraction, CS-KT attraction, CS-chromosome arm repulsion, and CS-CS attraction are combined. (F) Multipolar spindles develop when the CS-cortex attraction, CS-chromosome arm repulsion, and CS-CS attraction are combined but the CS-KT attraction is absent. To see this figure in color, go online.

cluster (so that all CSs belong to one interconnected cluster, and no chromosome is connected to this cluster).

Lastly, in the absence of the CS-KT attraction, repulsion of the CSs from the chromosome arms keeps the spindles multipolar even in the presence of the CS-CS attraction (Table S2). The bottom line is that the combination of the CS-KT attraction with CS-chromosome arm repulsion helps the bipolar spindles to emerge, but the bipolar architecture is not robust without interactions with the cell boundary.

Without inter-CS attraction, bipolarity does not emerge in cell confinement

Because the bipolar spindle architecture cannot be achieved without interactions with the cell boundary, we next turned to test the spindle mechanical equilibria in the cell confinement. We found that other than in the case of the CS-CS attraction, which we describe below, just confinement of the spindle in the cell has the same effect as the CS-cortex attraction (compare Figs. 3 and S1). Therefore, here we

only discuss the results in the presence of the CS-cortex attraction.

We find that spindles collapse in the presence of the CS-KT attraction and in the absence of the inter-CS interaction (Fig. 3 A), the same as in the unconfined case. The only effect of the CS-cortex attraction is that the collapsed spindle is located near the cortex. The collapse is not rescued by the addition of the CS-CS repulsion (Fig. 3 D), the same as in the unconfined case.

When we combine CS-KT attraction and CS-chromosome arm repulsion, the bipolar spindle geometry develops (Fig. 3 B), but not robustly: only ~40% of the spindles are bipolar. Thus, the presence of the attraction to the cortex does not make the bipolarity robust (compare with Fig. 2 B) in the absence of the CS-CS interactions. If we make the CS-CS interactions repulsive, then, as expected, all emerging spindles become multipolar (Fig. 3 E; Video S2).

Lastly, if only CS-chromosome arm repulsion is present, then, predictably and similar to the unconfined case, the multipolar spindles emerge either in the absence

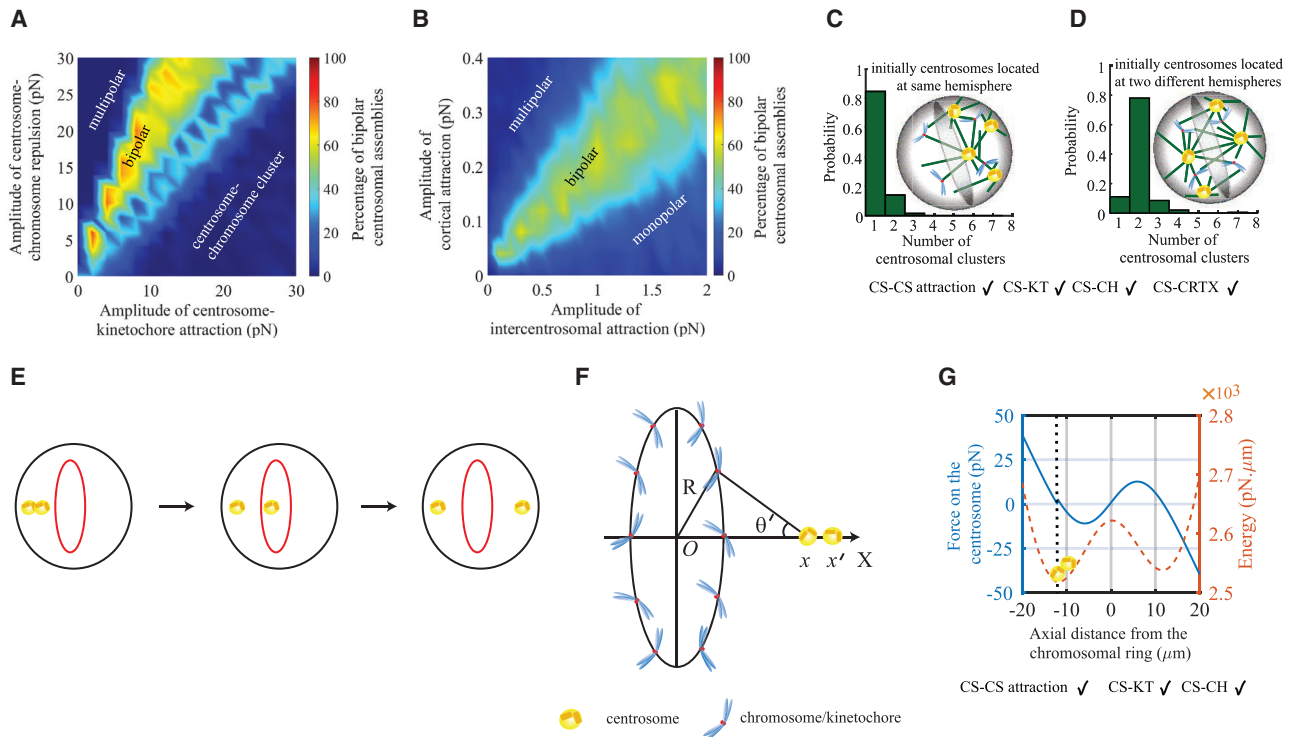


FIGURE 5 Bipolar CS clustering is sensitive to mechanical and structural parameters and initial conditions. In all simulations, forces or parameters other than varied ones are the same as those used in simulations for Fig. 4 E. (A) Percentage of the emerged bipolar spindle as the function of the amplitudes of the CS-KT attraction and CS-chromosome arm repulsion. (B) Percentage of the emerged bipolar spindle as the function of the amplitudes of the CS-cortex attraction and CS-CS attraction. (C and D) Relative frequencies of the CS cluster numbers when eight CSs are initially localized in the same (C) and different (D) hemispheres. (E) Scheme of the numerical experiment: the chromosomes are uniformly distributed along the circumference at the cell equator, and one CS is placed at the cell pole while another CS is gradually moved from that pole to the other one. (F) Coordinates and angles of the numerical experiment. (G) Force acting on the moving CS in the numerical experiment and respective energy of the system as a function of the inter-CS distance. To see this figure in color, go online.

(Fig. 3 C) or presence (Fig. 3 F) of the CS-CS repulsion. To conclude, the confinement and attraction of the CSs to the cortex does not make the bipolar spindle architecture robust.

Combination of the CS attraction to the cortex, to each other, and to KT with repulsion from the chromosomal arms makes the bipolar CS clustering robust

We finally tested the few remaining cases in which CS-CS attraction was present. We started with three cases of the spindle confined in the cell but the CSs not being attracted to the cortex and then explored the effect of the CS attraction to the cortex. Same as in the previously considered cases, in the absence of the CS-chromosome arm repulsion, the spindles collapsed in confinement (Fig. 4 A) and in the presence of the CS-cortex attraction (Fig. 4 D). Similarly, as in the previously considered cases, in the absence of the CS-KT attraction, multipolar spindles emerged in confinement (Fig. 4 C) and in the presence of the CS-cortex attraction (Fig. 4 F).

Eventually, we explored the combination of the CS-KT attraction, CS-chromosome arm repulsion, and CS-CS attraction, which promotes the bipolarity nonrobustly in the unconfined space (Fig. 2 F). We found that in confinement, the bipolarity becomes more robust: $\sim 60\%$ of the evolved spindles were bipolar (Fig. 4 B), compared to $\sim 40\%$ in the unconfined case. An even better result is achieved in the presence of the active CS-cortex attraction: in $\sim 80\%$ of cases, the CSs aggregated into two clusters (Fig. 4 E; Video S3), creating the familiar “doughnut” chromosome structure. The more robust bipolar CS clustering in this last case is due to the attraction of the evolving opposite CS clusters to the cortex that prevents them from falling onto each other, assisted by the repulsion from the chromosomal “doughnut.” We visually inspected the geometries of the chromosomal distributions in mono-, bi-, and multipolar spindles (Table S3) and found that the doughnut-like chromosome distribution is more characteristic of the bipolar spindles, whereas these distributions in mono- and multipolar spindles are more irregular. Similar conclusions were recently reached, both theoretically and experimentally, in (59).

Bipolar CS clustering is sensitive to mechanical, geometric, and structural parameters and initial conditions

Sensitivity to mechanical and structural parameters

To test how sensitive the spindle architecture is to the model parameters, we varied single and pairs of parameters, keeping the rest of the parameters equal to the base values listed in [Table S1](#) and repeated the simulations. Note that the base parameter values predict the robust bipolar spindles reported in [Fig. 4 E](#). We found that two force balances have to hold for the bipolarity. First, CS-KT attraction strength has to be proportional to the CS repulsion from the chromosome arms ([Fig. 5 A](#)); if the repulsion is weaker or stronger than the attraction, then the spindle collapses or becomes multipolar. Second, the strength of the CS-CS attraction has to be proportional to the CS-cortex attraction ([Fig. 5 B](#)); if the interaction with the cortex is weaker or stronger than the CS-CS attraction, then the spindle collapses or becomes multipolar. The sensitivity of the spindle architecture to the individual forces' strengths is further demonstrated in [Fig. S2, B and C](#).

Next, we investigated sensitivity to varying force ranges. Recall that the CS-KT attraction is distance independent in the model, and so there are three force ranges in the model—for the CS-chromosome arm repulsion and for the CS-CS and CS-cortex attractions. We varied these ranges and found that the range for the CS-chromosome arm repulsion has to be on the order of the cell radius ([Fig. S2 A](#)) for two CS clusters to emerge. The reason is rather simple: if this force range is too small, the repulsion is effectively too weak, and the spindle collapses. In the other limit, the repulsion is too strong, pushing the CSs into the cortex too hard for the CS-CS attraction to cluster them. On the other hand, the bipolarity is not very sensitive to the range of the CS-CS attraction ([Fig. S2 A](#)). Finally, we also varied the range of the CS-cortex attractions and found that this length has to be much smaller than the cell size for the bipolar spindles to emerge ([Fig. S4 C](#)). This can be explained if one considers the integrated effect of the whole cortex on one CS. It was demonstrated in several models (60) that if the range of the attraction to the cortex is long enough, then effectively, the force on the CS becomes centering. In that case, all CSs are pulled to the cell center, creating the monopolar spindle.

We investigated how the bipolar spindle length (pole-pole distance between two CS clusters) depends on various parameters ([Fig. S6](#)). We found that the spindle length slightly decreases with the growing CS number ([Fig. S6 B](#)) because of the CS-CS attraction but in general is not very sensitive to the CS and chromosome numbers ([Fig. S6, A and B](#)). The numbers of CSs in two poles, which depend on initial conditions, were not necessarily equal ([Fig. S6 F](#)), but the spindle length was insensitive to the CS number distribution ([Fig. S6 C](#)). The reason is that in the equilibrated spindle

in the model, the distance of the CS clusters from the chromosomal cluster is largely set by the balance of the CS-KT attraction and CS-CH repulsion, and the attraction between two CS clusters is too weak because these clusters are too far away from each other.

Lastly, we repeated all simulations for the cells with two CSs. As can be seen from [Fig. S3, C and D](#), proper bipolar architectures with the chromosomes between two segregated CSs emerge most robustly when there are either no CS-KT interactions or when CSs repel each other. This makes easy physical sense: two CSs segregate better when they repel, not attract, each other. The same conclusion was reached in several previous models (19,33,34). Other numerical tests are described in the [Supporting Materials and Methods](#).

Sensitivity to cell size and shape

We first investigated how the bipolarity, in the optimal case corresponding to [Fig. 4 E](#), depends on the size of a spherical cell ([Fig. S5 A](#)). We found that as the cell radius increases, the fraction of the monopolar spindles grows. This is easy to understand: the limit of large cells is equivalent to the unconfined case, in which the CS-CS attraction leads to CS aggregation into a single cluster. Interestingly, at an intermediate cell size, the fraction of multipolar spindles increases sharply ([Fig. S5 A](#)) because the attraction to the more expansive cortex allows space for more than two CS clusters to not “feel” each other. We also checked how the bipolarity depends on the elongation of one of the cell axes, whereas the other two are constant and equal ([Fig. S5 B](#)). We found that when one axis is much shorter than two others, the monopolar fraction increases, for the reason explained in the next paragraph. (For the same physical reason, when one axis elongates but two others shorten, keeping the cell volume constant ([Fig. S5 C](#)), the fraction of monopolar spindles increases: chromosomes spread from one elongated end of the cell to another, leaving the CSs too close to each other at the small circular cross section of the cell.) However, when one axis is much longer than two others, the multipolar fraction increases because the cortex area is too great, allowing the coexistence of multiple CS clusters. Importantly, this prediction is consistent with observations of Kwon et al. (5) that spherical cells form bipolar spindles, whereas elongated cells have more multipolar spindles. Noteworthy is that nonuniform, cell-geometry-dependent attraction to the cortex may be similarly responsible for the multipolarity observed in the experiments.

We repeated the simulations with parameters corresponding to the conditions most favorable for the spindle bipolarity ([Fig. 4 E](#)) in a drastically flattened cell ([Fig. S5, D–G](#)), with the volume equal to the volume of the basic cell shape. In the flat cell, the fraction of the bipolar spindles is significantly diminished. The reasons are twofold: first, clusters of the chromosomes sometimes span the space

between the virtually flat proximal cell surfaces so that CSs do not have sufficient space to navigate around these clusters and thus fail to reach other CSs, which promotes multipolarity. Second, when a bipolar spindle does emerge, the chromosomal doughnut aligns with the large radius of the flattened cell (around the equator), whereas the two CS clusters reside at the “north and south poles” (at the opposite ends of the shortest axis of the cell). Because in this configuration, the distance between the poles is small, the two-cluster attraction is too strong and the repulsive effect of the chromosomal arms barrier is too weak because the cell equator is too far from its poles. These results may be relevant for understanding the reason for the rounding up of mitotic cells (61).

We also investigated how the spindle length depended on the cell size and shape when the spindle is bipolar (Fig. S6, *D* and *E*). We found that in the spherical cell, the spindle length scales with the cell size in small cells, but then, curiously, after reaching a maximum for the cell with a radius 30 μm , decreases to a cell-size-independent length for larger cells (Fig. S6 *D*). The reason is that, according to the model, two CS clusters are kept near the opposite poles of the cell by the attraction to the cortex in smaller cells, whereas in larger cells, the cortex attraction fails to stretch the spindle against the internal force balance. Similar scaling (without the maximum at an intermediate cell size) was observed (reviewed in (62)); however, multiple complex mechanisms, not just simple mechanics, are responsible for the scaling. This effect depends not only on the size but also on the shape of the cell (Fig. S6 *E*).

Sensitivity to the initial conditions

How important is it where the CSs are placed initially, at the end of prophase—early prometaphase? We simulated two scenarios: first, the CSs were scattered uniformly across the whole cell; second, the CSs were located with uniform probability only in half (one hemisphere) of the cell. Fig. 5, *C* and *D* show that in the first case, the bipolar spindle evolves, whereas in the second case, the monopolar one does. The explanation is that if initially the CSs are close together, their attraction overcomes the repulsion of a small number of the chromosome arms between the individual CSs. Thus, the proper spindle architecture is sensitive not only to the mechanical parameters but also to the initial conditions. The same conclusion holds for the cell with two (Fig. S4, *E* and *F*) or more CSs, including both even and odd number of CSs (Fig. S7, *A* and *B*).

Mechanical energy landscape of the bipolar spindle

To have a better understanding of the spindle bipolarity, we considered a simple analytical model, mimicking the proper spindle geometry: the chromosomes arranged uniformly in an annular-shaped ring of inner radius r_a and outer radius r_b (Table S1) within a spherical cell of radius R_{cell} (Fig. 5, *E* and *F*). Two CSs are positioned on the axis through the

center of the ring, perpendicular to the plane of the ring. In the presence of the CS-chromosome arm repulsion and CS-KT and CS-CS attraction, we calculated (Supporting Materials and Methods) the configuration's energy as a function of the CS-CS distance when one CS is at the left from the chromosomal ring and another moves to the right along the axis. Fig. S4 *H* shows that when there is no CS-CS interaction, there is a double-well energy profile for this spindle, with equally deep energy wells. Each well corresponds to a CS being at a mechanically equilibrium distance from the chromosomal ring, at which the CS-KT and CS-chromosome arm forces are balanced to zero. Because the CSs do not interact in this case, the monopolar and bipolar spindles have the same energies, with a significant energy barrier between them, because of the difficulty of pushing the CS through the chromosomal ring. If we add the CS-CS attraction, the double-well energy profile changes, with the well corresponding to the monopolar spindle becoming deeper than the well corresponding to the bipolar spindle (Fig. 5 *G*). This explains why the monopolar spindles are the most stable (see the Supporting Materials and Methods); however, the bipolar spindle is very stable as well because the energy barrier between them remains significant. Similar conclusions were recently reached in (59). Lastly, this result also illustrates the predicted sensitivity to the initial conditions: if we start with both CSs to the left from the chromosomes, they both “fall” into the same energy well, making the monopolar spindle, but if initially, the CSs are at the opposite sides of the chromosomes, they each “fall” into their own energy well, making the bipolar spindle.

DISCUSSION

In this study, we examined computationally mechanical requirements for the bipolar CS clustering and reached the following conclusions. Four types of forces are necessary for the bipolar spindle architecture: CS attraction to each other, to the KTs, and to the cortex and CS repulsion from the chromosome arms. For these forces to be sufficient for the bipolarity, four further conditions have to be met: CS attraction to each other needs to be proportional to the attraction to the cell cortex, CS attraction to the KTs has to be proportional to the repulsion from the chromosome arms, interactions of the CSs with both KTs and chromosome arms have to be on the scale of the cell size, and CS attraction to the cortex has to be short-ranged. The physical explanation of the bipolarity under these conditions is this: the balance of the constant attraction to the KTs and repulsion from the chromosome arms decreasing with distance on the scale of the cell places CSs at certain equilibrium distance from the chromosomes, and this equilibrium distance is on the order of the cell size. If CSs attract each other and attraction to the cortex is strong near the cortex, then, providing that initially the CSs are scattered around the

cell, proximal CSs start clustering into greater and greater clusters, and at some point, there is one cluster in one hemisphere of the cell and another one in another hemisphere. Most of the chromosomes trying to stay away from both CS clusters are in the middle, creating a barrier for the CS clusters; in addition, the cortex pulls two CS clusters into the opposite directions, stabilizing the bipolarity. If the attraction to the cortex is global, nothing can prevent the collapse of the two clusters.

The simulations, interestingly, successfully reproduce the characteristic “doughnut-like” spatial organization of chromosomes in prometaphase (63). The physical explanation is that for chromosomes staying away from two opposite CS clusters at the cell poles, the doughnut around the cell equator is the place where all chromosomes are at equilibrium distance from the cell poles.

If CSs attract each other but the interactions with the cortex are weak, CSs cluster into one group at the cell center, chromosomes spread over the cortical surface, and the monopolar spindle emerges. If, on the other hand, the interactions with the cortex are weak but CSs repel each other (or do not interact with each other), the chromosomes gather at the center, whereas CSs spread randomly over the cortex, making the multipolar spindle. Also, if there is no connection between the KTs and CSs, the spindle is multipolar. Both mono- and multipolar spindles were observed. Finally, without the repulsion from the chromosome arms, the whole spindle collapses; this, to our knowledge, was never observed, perhaps because there is always some repulsion from the chromosome arms.

Our model predictions are in general qualitative agreement with the published data: minus-end motors dynein (13) and kinesin-14 (5,12), normally associated with attractive forces in multiple models, are needed for CS clustering, suggesting that both attractions of CSs to the cortex and each other are necessary. Higher activity of the plus-end kinesin-5 motor, normally associated with repulsive forces in multiple models, diminishes the clustering effect (64). Perturbations of chromokinesins that contribute to the repulsion of the CSs from the chromosome arms leads to spindle defects (65,66). A number of studies suggested that MTs, MT-associated proteins, and motors, affecting not only cortex and CS-CS forces but also CS-KT forces, contribute to clustering (5,13,67,68). This is in agreement with the prediction that magnitude of the CS-KT attraction affects the clustering effect (Fig. 5 A; Fig. S2 B). A few studies demonstrated that although inactivation of one type of motor disrupts spindle morphology, the phenotype can be rescued by simultaneous inactivation of another, opposing motor (69–71). Such pairwise inactivation of opposite motors is likely to diminish two opposing forces while keeping their ratio unchanged, and so the stability of the spindle morphology under such double perturbations is consistent with the model. CSs that lack chromosomes between them do not form a stable spindle-like MT array (72), in agreement with the model.

The predicted sensitivity to the initial conditions—defects in the spindle architecture when the CSs are initially too close to each other—was documented in (73).

It was shown that if the interaction of CSs with the cortex is not uniform, but rather CSs attract local patches on the cortex, which is the case for cells with anisotropic and heterogeneous adhesion patterns, then multipolarity of the spindle is enhanced (5,16,17). Though we have not simulated such a situation explicitly (this is a worthy future effort), qualitatively, it is clear that more than two localized adhesive patches would attract locally smaller CS clusters, preventing them from merging into bigger ones. The model also gives insight into the nontrivial role of cell shape in positioning and shaping the spindle (74).

It is thought-provoking to explore the progression of the spindle through stages of mitosis from the model’s point of view. There are no MT-KT connections in early prometaphase, so the model says that at this stage, the spindles in multi-CS cells are multipolar. Later, when enough MT-KT connections are made, CS clustering follows. Interestingly, multipolar spindles in early prometaphase and CS clusters in late prometaphase actually were observed in *Drosophila* SakOE neuroblast spindles (75), in agreement with the prediction. This sequence of events, in fact, could enforce initial conditions benefitting later bipolarity by pushing apart CSs at the early stage, preventing all of them from ending up in the same hemisphere of the cell.

Molecular mechanisms underlying proportional scaling of the opposing pairs of forces in the spindle, each of which depends on many independent factors such as motor and MT densities and organelle sizes, remain elusive. Many various combinations of molecular motors can generate forces necessary for the bipolar CS clustering. To explore relevant molecular pathways deeper, agent-based modeling will be needed. Such stochastic modeling will also circumvent the problem of choosing “temperature” in our energy-minimization approach: the temperatures associated with the heat bath in the Monte Carlo simulation algorithm are manifestations of stochastic fluctuations arising from the MT dynamic instability and finite numbers and stochastic dynamics of the motors. Besides stochastic effects, other aspects of the spindle mechanics will have to be considered to make the model less simplistic. Those include the influence of merotelic errors of assembly on the force balance (25), space-dependent motor regulation (15), viscoelastic properties of the spindle (23), anisotropy of the MT asters around CSs (40,76), and role of the cortex flow in bringing CSs together (77), not to mention biophysical details of the magnitudes and spatial dependencies of the forces in the spindle that remain under-researched (22,47,78).

The predicted conditions for the spindle bipolarity in multi-CS cells are stringent, including proportionality of two pairs of forces as well as strict limits on the ranges of these forces. (It is worth noting that the proportionality of pairs of opposing forces was also predicted for length

regulation of spindles in the early *Drosophila* embryo (34).) These predicted scaling and force ranges probably indicate that multiple mechanochemical feedbacks, the molecular nature of which is unknown, robustly regulate the mechanical parameters to satisfy exactly these conditions. Another possibility is that additional mechanisms are in place to make the bipolar CS clustering more robust. One distinct possibility is that CSs are not equal; our model suggests that the robust bipolar spindle emerges in two-CS cells when these CSs repel each other. If these two CSs are made “dominant,” whereas other CSs are “inactivated,” or if CSs are attracted not individually to each other, but rather to poles of a dominant interpolar MT bundle (both ideas are reviewed in (4)), then the bipolar spindle could emerge more robustly. Yet another factor that could enhance the robustness is a nonisotropic CS-cortex interaction. Last, but not least, there is no “the” spindle: different cell types evolved to use differently the common molecular toolbox to build bipolar spindles (79). Comparing design principles behind different mechanisms to cluster multiple CSs in mitosis is one of the future goals.

CONCLUSIONS

To assemble the bipolar spindle in a multicentrosomal cell, the CSs have to attract proportionally to each other and to the cell cortex; also, CSs need to have a proportional attraction to the KTs and repulsion from the chromosome arms. In addition, the CS-cortex interaction has to be short-ranged, whereas the ranges of the CS-KT and CS-chromosome arm interactions have to be comparable with the cell size. Without CS-chromosome arm repulsion, the spindles collapse. Without CSs being attracted to the cortex, monopolar spindles evolve if CSs mutually attract and multipolar spindles if CSs do not interact or repel each other. Spindle architecture is sensitive to initial conditions.

SUPPORTING MATERIAL

Supporting Material can be found online at <https://doi.org/10.1016/j.bpj.2020.06.004>.

AUTHOR CONTRIBUTIONS

A.M. and R.P. conceived and directed the study with help from A.K. S.C., A.M., and R.P. wrote the manuscript with help from A.K. S.C., A.S., and R.P. developed the methods. All authors analyzed the data.

ACKNOWLEDGMENTS

We thank C. Miles for useful discussions and help with the manuscript and M. Kwon for attracting our attention to the problem of centrosomal clustering.

S.C. and A.S. were supported by fellowships from the University Grants Commission, India. R.P. acknowledges grant no. EMR/2017/001346 of

SERB, DST, India for the computational facility. A.M. was supported by the National Institutes of Health grant GM121971 and by the National Science Foundation grant DMS1953430. A.K. was supported by the National Institutes of Health grant GM130298.

REFERENCES

- Rafelski, S. M., and W. F. Marshall. 2008. Building the cell: design principles of cellular architecture. *Nat. Rev. Mol. Cell Biol.* 9:593–602.
- Karsenti, E., and I. Vernos. 2001. The mitotic spindle: a self-made machine. *Science.* 294:543–547.
- Meunier, S., and I. Vernos. 2016. Acentrosomal microtubule assembly in mitosis: the where, when, and how. *Trends Cell Biol.* 26:80–87.
- Marthiens, V., M. Piel, and R. Basto. 2012. Never tear us apart—the importance of centrosome clustering. *J. Cell Sci.* 125:3281–3292.
- Kwon, M., S. A. Godinho, ..., D. Pellman. 2008. Mechanisms to suppress multipolar divisions in cancer cells with extra centrosomes. *Genes Dev.* 22:2189–2203.
- Nigg, E. A. 2002. Centrosome aberrations: cause or consequence of cancer progression? *Nat. Rev. Cancer.* 2:815–825.
- Faggioli, F., P. Vezzoni, and C. Montagna. 2011. Single-cell analysis of ploidy and centrosomes underscores the peculiarity of normal hepatocytes. *PLoS One.* 6:e26080.
- Doxsey, S. 2001. Re-evaluating centrosome function. *Nat. Rev. Mol. Cell Biol.* 2:688–698.
- Acilan, C., and W. S. Saunders. 2008. A tale of too many centrosomes. *Cell.* 134:572–575.
- Silkworth, W. T., I. K. Nardi, ..., D. Cimini. 2009. Multipolar spindle pole coalescence is a major source of kinetochore mis-attachment and chromosome mis-segregation in cancer cells. *PLoS One.* 4:e6564.
- Ganem, N. J., S. A. Godinho, and D. Pellman. 2009. A mechanism linking extra centrosomes to chromosomal instability. *Nature.* 460:278–282.
- Basto, R., K. Brunk, ..., J. W. Raff. 2008. Centrosome amplification can initiate tumorigenesis in flies. *Cell.* 133:1032–1042.
- Quintyne, N. J., J. E. Reing, ..., W. S. Saunders. 2005. Spindle multipolarity is prevented by centrosomal clustering. *Science.* 307:127–129.
- Dumont, S., and T. J. Mitchison. 2009. Force and length in the mitotic spindle. *Curr. Biol.* 19:R749–R761.
- Maiato, H., A. M. Gomes, ..., M. Barisic. 2017. Mechanisms of chromosome congression during mitosis. *Biology (Basel).* 6:13.
- Théry, M., V. Racine, ..., M. Bornens. 2005. The extracellular matrix guides the orientation of the cell division axis. *Nat. Cell Biol.* 7:947–953.
- Théry, M., A. Jiménez-Dalmaroni, ..., F. Jülicher. 2007. Experimental and theoretical study of mitotic spindle orientation. *Nature.* 447:493–496.
- Kapoor, T. M., T. U. Mayer, ..., T. J. Mitchison. 2000. Probing spindle assembly mechanisms with monastrol, a small molecule inhibitor of the mitotic kinesin, Eg5. *J. Cell Biol.* 150:975–988.
- Ferenz, N. P., R. Paul, ..., P. Wadsworth. 2009. Dynein antagonizes eg5 by crosslinking and sliding antiparallel microtubules. *Curr. Biol.* 19:1833–1838.
- Leary, A., S. Sim, ..., J. Vogel. 2019. Successive kinesin-5 microtubule crosslinking and sliding promote fast, irreversible formation of a stereotyped bipolar spindle. *Curr. Biol.* 29:3825–3837.e3.
- Maiato, H., and E. Logarinho. 2014. Mitotic spindle multipolarity without centrosome amplification. *Nat. Cell Biol.* 16:386–394.
- Ferraro-Gideon, J., R. Sheykhan, ..., A. Forer. 2013. Measurements of forces produced by the mitotic spindle using optical tweezers. *Mol. Biol. Cell.* 24:1375–1386.

23. Takagi, J., T. Itabashi, ..., S. Ishiwata. 2014. Micromechanics of the vertebrate meiotic spindle examined by stretching along the pole-to-pole axis. *Biophys. J.* 106:735–740.
24. Minc, N., D. Burgess, and F. Chang. 2011. Influence of cell geometry on division-plane positioning. *Cell.* 144:414–426.
25. Gay, G., T. Courtheoux, ..., Y. Gachet. 2012. A stochastic model of kinetochore-microtubule attachment accurately describes fission yeast chromosome segregation. *J. Cell Biol.* 196:757–774.
26. Pavin, N., and I. M. Tolić. 2016. Self-organization and forces in the mitotic spindle. *Annu. Rev. Biophys.* 45:279–298.
27. Zaytsev, A. V., D. Segura-Peña, ..., E. L. Grishchuk. 2016. Bistability of a coupled Aurora B kinase-phosphatase system in cell division. *eLife.* 5:e10644.
28. Elting, M. W., M. Prakash, ..., S. Dumont. 2017. Mapping load-bearing in the mammalian spindle reveals local kinetochore fiber anchorage that provides mechanical isolation and redundancy. *Curr. Biol.* 27:2112–2122.e5.
29. Varshney, N., S. Som, ..., K. Sanyal. 2019. Spatio-temporal regulation of nuclear division by Aurora B kinase Ipl1 in *Cryptococcus neoformans*. *PLoS Genet.* 15:e1007959.
30. Li, J., L. Cheng, and H. Jiang. 2019. Cell shape and intercellular adhesion regulate mitotic spindle orientation. *Mol. Biol. Cell.* 30:2458–2468.
31. Letort, G., I. Bennabi, ..., M. E. Terret. 2019. A computational model of the early stages of acentriolar meiotic spindle assembly. *Mol. Biol. Cell.* 30:863–875.
32. Lamson, A. R., C. J. Edelmaier, ..., M. D. Betterton. 2019. Theory of cytoskeletal reorganization during cross-linker-mediated mitotic spindle assembly. *Biophys. J.* 116:1719–1731.
33. Nédélec, F. 2002. Computer simulations reveal motor properties generating stable antiparallel microtubule interactions. *J. Cell Biol.* 158:1005–1015.
34. Wollman, R., G. Civelekoglu-Scholey, ..., A. Mogilner. 2008. Reverse engineering of force integration during mitosis in the *Drosophila* embryo. *Mol. Syst. Biol.* 4:195.
35. Rubinstein, B., K. Larripa, ..., A. Mogilner. 2009. The elasticity of motor-microtubule bundles and shape of the mitotic spindle. *Phys. Biol.* 6:016005.
36. Odell, G. M., and V. E. Foe. 2008. An agent-based model contrasts opposite effects of dynamic and stable microtubules on cleavage furrow positioning. *J. Cell Biol.* 183:471–483.
37. Manhart, A., S. Windner, ..., A. Mogilner. 2018. Mechanical positioning of multiple nuclei in muscle cells. *PLoS Comput. Biol.* 14:e1006208.
38. Graner, F., and J. A. Glazier. 1992. Simulation of biological cell sorting using a two-dimensional extended Potts model. *Phys. Rev. Lett.* 69:2013–2016.
39. Pearson, C. G., M. K. Gardner, ..., K. Bloom. 2006. Measuring nanometer scale gradients in spindle microtubule dynamics using model convolution microscopy. *Mol. Biol. Cell.* 17:4069–4079.
40. Lacroix, B., G. Letort, ..., J. Dumont. 2018. Microtubule dynamics scale with cell size to set spindle length and assembly timing. *Dev. Cell.* 45:496–511.e6.
41. Paul, R., R. Wollman, ..., A. Mogilner. 2009. Computer simulations predict that chromosome movements and rotations accelerate mitotic spindle assembly without compromising accuracy. *Proc. Natl. Acad. Sci. USA.* 106:15708–15713.
42. Sutradhar, S., S. Basu, and R. Paul. 2015. Intercentrosomal angular separation during mitosis plays a crucial role for maintaining spindle stability. *Phys. Rev. E Stat. Nonlin. Soft Matter Phys.* 92:042714.
43. Som, S., S. Chatterjee, and R. Paul. 2019. Mechanistic three-dimensional model to study centrosome positioning in the interphase cell. *Phys. Rev. E.* 99:012409.
44. Joglekar, A. P., and A. A. Kukreja. 2017. How kinetochore architecture shapes the mechanisms of its function. *Curr. Biol.* 27:R816–R824.
45. Dietz, R. 1972. Anaphase behaviour of inversions in living crane-fly spermatocytes. *Chromosom. Today.* 3:70–85.
46. Khodjakov, A., and C. L. Rieder. 1996. Kinetochores moving away from their associated pole do not exert a significant pushing force on the chromosome. *J. Cell Biol.* 135:315–327.
47. Brouhard, G. J., and A. J. Hunt. 2005. Microtubule movements on the arms of mitotic chromosomes: polar ejection forces quantified in vitro. *Proc. Natl. Acad. Sci. USA.* 102:13903–13908.
48. Ke, K., J. Cheng, and A. J. Hunt. 2009. The distribution of polar ejection forces determines the amplitude of chromosome directional instability. *Curr. Biol.* 19:807–815.
49. Ye, A. A., J. Deretic, ..., T. J. Maresca. 2015. Aurora A kinase contributes to a pole-based error correction pathway. *Curr. Biol.* 25:1842–1851.
50. Drpic, D., A. J. Pereira, ..., H. Maiato. 2015. Polar ejection forces promote the conversion from lateral to end-on kinetochore-microtubule attachments on mono-oriented chromosomes. *Cell Rep.* 13:460–468.
51. Waters, J. C., R. W. Cole, and C. L. Rieder. 1993. The force-producing mechanism for centrosome separation during spindle formation in vertebrates is intrinsic to each aster. *J. Cell Biol.* 122:361–372.
52. Laan, L., S. Roth, and M. Dogterom. 2012. End-on microtubule-dynein interactions and pulling-based positioning of microtubule organizing centers. *Cell Cycle.* 11:3750–3757.
53. Letort, G., F. Nédélec, ..., M. Théry. 2016. Centrosome centering and dcentering by microtubule network rearrangement. *Mol. Biol. Cell.* 27:2833–2843.
54. Mogilner, A., L. Edelstein-Keshet, ..., A. Spiros. 2003. Mutual interactions, potentials, and individual distance in a social aggregation. *J. Math. Biol.* 47:353–389.
55. Holmes-Cerfon, M., S. J. Gortler, and M. P. Brenner. 2013. A geometrical approach to computing free-energy landscapes from short-ranged potentials. *Proc. Natl. Acad. Sci. USA.* 110:E5–E14.
56. Chang, A. Y., and W. F. Marshall. 2019. Dynamics of living cells in a cytomorphological state space. *Proc. Natl. Acad. Sci. USA.* 116:21556–21562.
57. Kolokolnikov, T., H. Sun, ..., A. L. Bertozzi. 2011. Stability of ring patterns arising from two-dimensional particle interactions. *Phys. Rev. E Stat. Nonlin. Soft Matter Phys.* 84:015203.
58. Ben-Isaac, E., Y. Park, ..., Y. Shokef. 2011. Effective temperature of red-blood-cell membrane fluctuations. *Phys. Rev. Lett.* 106:238103.
59. Goupil, A., M. Nano, ..., R. Basto. 2020. Chromosomes function as a barrier to mitotic spindle bipolarity in polyploid cells. *J. Cell Biol.* 219:e201908006.
60. Dmitrieff, S., and N. Minc. 2019. Scaling properties of centering forces. *Europhys. Lett.* 125:48001.
61. Lancaster, O. M., M. Le Berre, ..., B. Baum. 2013. Mitotic rounding alters cell geometry to ensure efficient bipolar spindle formation. *Dev. Cell.* 25:270–283.
62. Wesley, C. C., S. Mishra, and D. L. Levy. 2020. Organelle size scaling over embryonic development. *Wiley Interdiscip. Rev. Dev. Biol.* 31:e375.
63. Magidson, V., R. Paul, ..., A. Khodjakov. 2015. Adaptive changes in the kinetochore architecture facilitate proper spindle assembly. *Nat. Cell Biol.* 17:1134–1144.
64. Drosopoulos, K., C. Tang, ..., S. Linardopoulos. 2014. APC/C is an essential regulator of centrosome clustering. *Nat. Commun.* 5:3686.
65. Takagi, J., T. Itabashi, ..., S. Ishiwata. 2013. Chromosome position at the spindle equator is regulated by chromokinesin and a bipolar microtubule array. *Sci. Rep.* 3:2808.
66. Mazumdar, M., S. Sundareshan, and T. Misteli. 2004. Human chromokinesin KIF4A functions in chromosome condensation and segregation. *J. Cell Biol.* 166:613–620.
67. Leber, B., B. Maier, ..., A. Krämer. 2010. Proteins required for centrosome clustering in cancer cells. *Sci. Transl. Med.* 2:33ra38.

68. Morris, E. J., E. Kawamura, ..., S. Dedhar. 2017. Stat3 regulates centrosome clustering in cancer cells via Stathmin/PLK1. *Nat. Commun.* 8:15289.
69. Gaglio, T., A. Saredi, ..., D. A. Compton. 1996. Opposing motor activities are required for the organization of the mammalian mitotic spindle pole. *J. Cell Biol.* 135:399–414.
70. Mountain, V., C. Simerly, ..., D. A. Compton. 1999. The kinesin-related protein, HSET, opposes the activity of Eg5 and cross-links microtubules in the mammalian mitotic spindle. *J. Cell Biol.* 147:351–366.
71. Ganem, N. J., and D. A. Compton. 2004. The KinI kinesin Kif2a is required for bipolar spindle assembly through a functional relationship with MCAK. *J. Cell Biol.* 166:473–478.
72. Faruki, S., R. W. Cole, and C. L. Rieder. 2002. Separating centrosomes interact in the absence of associated chromosomes during mitosis in cultured vertebrate cells. *Cell Motil. Cytoskeleton.* 52:107–121.
73. Silkworth, W. T., I. K. Nardi, ..., D. Cimini. 2012. Timing of centrosome separation is important for accurate chromosome segregation. *Mol. Biol. Cell.* 23:401–411.
74. Lázaro-Diéíguez, F., I. Ispolatov, and A. Müsch. 2015. Cell shape impacts on the positioning of the mitotic spindle with respect to the substratum. *Mol. Biol. Cell.* 26:1286–1295.
75. Morin, X., R. Daneman, ..., W. Chia. 2001. A protein trap strategy to detect GFP-tagged proteins expressed from their endogenous loci in *Drosophila*. *Proc. Natl. Acad. Sci. USA.* 98:15050–15055.
76. Redemann, S., J. Baumgart, ..., T. Müller-Reichert. 2017. *C. elegans* chromosomes connect to centrosomes by anchoring into the spindle network. *Nat. Commun.* 8:15288.
77. Rhys, A. D., P. Monteiro, ..., S. A. Godinho. 2018. Loss of E-cadherin provides tolerance to centrosome amplification in epithelial cancer cells. *J. Cell Biol.* 217:195–209.
78. Nicklas, R. B. 1983. Measurements of the force produced by the mitotic spindle in anaphase. *J. Cell Biol.* 97:542–548.
79. Farhadifar, R., C. F. Baer, ..., D. J. Needleman. 2015. Scaling, selection, and evolutionary dynamics of the mitotic spindle. *Curr. Biol.* 25:732–740.

Supporting Material

Mechanics of multi-centrosomal clustering in bipolar mitotic spindles

S Chatterjee, A Sarkar, J Zhu, A Khodjakov, A Mogilner, R Paul

Additional examination of the model behavior

We explored the influence of an additional CS-CS force with the length-dependence different from the exponential one: it was shown theoretically that when antiparallel MTs emanating from two CSs overlap, and crosslinking molecular motors at the overlap initiate MT sliding, that the resulting force $f_{overlap}$ and corresponding potential energy of moving a CS from distance r_1 to r_2 keeping the other CS fixed are :

$$f_{overlap} = f_{overlap}^{(0)} r e^{-r/L_1}, \quad \Delta E_{CS-CS} = -f_{overlap}^{(0)} \int_{r_1}^{r_2} r e^{-r/L_1} dr. \quad (S1)$$

We tested what happens if the CSs interact by a combination of the attractive and repulsive forces. The former can arise when MTs from one CS are reeled in by minus-end directed Dynein motors on another CS. The latter can be generated by plus-end directed Kinesin-5 motors on the antiparallel overlaps between the MTs extending from the interacting CSs. In the first case, the attractive force decreases with distance exponentially, while in the second case, the force is small at small and great distances and is maximal at an intermediate distance. As expected, there has to be a linearly proportional balance between the attractive and repulsive forces for the bipolar spindle to emerge (Fig. S4A, B). If instead of plus-end directed Kinesin-5 motors, minus-end directed Kinesin-14 motors are dominant at the MT overlaps, then forces generated by both Dynein and Kinesin-14 become attractive, but their distance-dependencies are different. In that case, the motors complement each other: if one is weaker, another one has to be stronger for the bipolar spindle to emerge (Fig. S4D).

The bipolar spindles emerge under many different force combinations, albeit with different frequencies. We tested how the length (pole-to-pole distance) of these spindles depended on the force combinations. Fig. S3A, B demonstrates that to have a proper spindle length (comparable with the cell size), the only condition is that CS-chromosome arm repulsion must be present; other forces do not matter. (They, of course, affect the probability of the bipolarity.) This is one more demonstration of the crucial role of the CS-chromosome arm repulsion.

Chromosome number varies depending on the cell type, and so we explored how the bipolarity depends on the chromosome number. We found that the percentage of bipolar spindles decreases with the decreasing chromosome number (Fig. S2D). The reason is that smaller numbers of chromosome arms do not repel the CSs strong enough lowering the energy barrier between the mono- and bipolar configurations. Another reason is that stochastic effects increase with the decreasing number of interacting bodies, effectively enhancing the probability of converging to the lowest energy, monopolar configuration.

Calculation of energy for different spindle configurations

Each of the evolved spindles corresponds to a local minimum in the mechanical energy landscape. We took all mono-, bi- and multipolar spindles evolved in the simulations with various force combinations, and computed the mechanical energies of each respective configuration of CSs and chromosomes obtained at the end of each stochastic simulations by using the following algorithm. As the chromosomes do not interact with each other, except by the steric repulsion, we start with the chromosomes distributed in the cell exactly as they are at the end of a simulation, with no CSs in the cell, and assign zero energy to this initial condition. Let $\{r_i\}$ be the position of the CSs and $\{d_{ij}\}$ to be the Euclidean distance between two CSs positioned at r_i and r_j respectively at the end of the simulation. We then bring the CSs one by one from ∞ to r_i .

1. The following algorithm is used to evaluate the total energy due to the inter-CS attraction.
 - a. We evaluate the potential energy of bringing the i^{th} CS from ∞ to r_i in presence of other $(i - 1)$ CSs which are kept fixed at

their individual locations as follows:

$$\Delta E_i = - \sum_{j=1}^{i-1} \int_{\infty}^{d_{ij}} f_{CS-CS}^{(0)} e^{-r/L_1} dr. \quad (S2)$$

b. We perform the same task for all CSs and compute the net energy by summing over all the ΔE_i s. Note that if ΔE_{ij} is the energy of interactions of i^{th} and j^{th} CSs, this algorithm gives us the sum of all pairwise interaction energies as follows:

$$\sum_{i=2}^{N_{CS}} \sum_{j=1}^{i-1} \Delta E_{CS-CS}^{ij} = - \sum_{i=2}^{N_{CS}} \sum_{j=1}^{i-1} \int_{\infty}^{d_{ij}} f_{CS-CS}^{(0)} e^{-r/L_1} dr \quad (S3)$$

2. We evaluate the total energy of the CS-KT attraction as follows:

$$\sum_{i=1}^{N_{CS}} \sum_{j=1}^{N_{KT}} \Delta E_{CS-KT}^{ij} = - \sum_{i=1}^{N_{CS}} \sum_{j=1}^{N_{CH}} \int_{d_c}^{d_{CS-CH}^{ij}} f_{CS-KT}^{(0)} dr. \quad (S4)$$

Here, d_{CS-CH}^{ij} is the distance between the i^{th} CS and the j^{th} chromosome. As the CS-KT attraction is constant and acting only inside the cell, the cutoff distance, d_c , for the effective CS-KT attraction is chosen as the diameter of the cell. As we have the elliptical cell with semi-major and semi-minor axes 20, 15, 15 μm , we considered the cutoff distance $d_c = 2 \times 20 \mu\text{m} = 40 \mu\text{m}$ in the simulation.

3. We evaluate the total energy of the CS-chromosome arm repulsion as follows:

$$\sum_{i=1}^{N_{CS}} \sum_{j=1}^{N_{CH}} \Delta E_{CS-CH}^{ij} = - \sum_{i=1}^{N_{CS}} \sum_{j=1}^{N_{CH}} \int_{\infty}^{d_{CS-CH}^{ij}} f_{CS-CH}^{(0)} e^{-r/L_1} dr. \quad (S5)$$

4. We evaluate the total energy of the CS-cortex attraction as follows:

$$\sum_{i=1}^{N_{CS}} \Delta E_{CS-CRTX}^i = - \sum_{i=1}^{N_{CS}} \int_{\Omega} ds \int_{\infty}^{d_{CS-CRTX}^{(i)}(s)} f_{CS-CRTX}^{(0)} e^{-r/L_2} dr. \quad (S6)$$

Here, $d_{CS-CRTX}^{(i)}(s)$ is the distance between i^{th} CS and the point with coordinate s on the cortex.

The average computed energies are reported in Fig. S4G. There are two nontrivial lessons from Fig. S4G: first, the energy differences, under any given force combination, between mono-, bi- and multipolar spindles are much smaller than the average energy of all spindles under given conditions. This does not mean that the cell can easily change the spindle geometry or that significant stochasticity can destabilize the spindle because energy barriers between the spindles could be significant. The second lesson is that under all but one condition, the monopolar spindle has the lowest energy (which does not necessarily mean that such spindle is the most stable), followed by the bipolar, and the multipolar spindle. The only case when the bipolar spindle has the lowest energy is when the forces of the CS-CS and CS-cortex attractions are absent.

Analysis of the energy change upon continuous shift of one CS along the spindle axis and through the ring of chromosomes

We consider the chromosomes to be spatially organized in an annular shaped ring of inner radius r_a and outer radius r_b (Table S1) within a spherical cell of radius R_{cell} (Table S1). Two CSs are placed on the axis through the center of the ring, perpendicular to the plane into which the ring is embedded into. The chromosome density in the annular ring can be written as $\rho_{ch} = N_{ch}/[\pi(r_b^2 - r_a^2)]$. The CS-chromosome arm repulsion can be evaluated as follows:

$$\begin{aligned} \vec{f}_{CS-CH}^{rep}(x) &= \int_0^{2\pi} \int_{r_a}^{r_b} \rho_{ch} R d\theta dR f_{CS-CH}(r) \cos \theta' \\ &= 2\pi \rho_{ch} \int_{r_a}^{r_b} R f_{CS-CH}(r) \cos \theta' dR \\ &= 2\pi \rho_{ch} f_{CS-CH}^{(0)} \int_{r_a}^{r_b} e^{-\sqrt{R^2+x^2}/L_1} \frac{x}{\sqrt{R^2+x^2}} dR \\ &= 2\pi \rho_{ch} f_{CS-CH}^{(0)} x L_1 \left[e^{-\sqrt{r_a^2+x^2}/L_1} - e^{-\sqrt{r_b^2+x^2}/L_1} \right]. \end{aligned} \quad (S7)$$

The energy to bring over a CS from ∞ to x under the influence of the above mentioned force field is:

$$\begin{aligned}
E_{CS-CH}^{rep}(x) &= - \int_{\infty}^x 2\pi\rho_{ch}f_{CS-CH}^{(0)}L_1 \left[xe^{-\sqrt{r_a^2+x^2}/L_1} - xe^{-\sqrt{r_b^2+x^2}/L_1} \right] dx \\
&= -2\pi\rho_{ch}f_{CS-CH}^{(0)}(L_1)^2 \left[e^{-\sqrt{r_b^2+x^2}/L_1} \left(\sqrt{r_b^2+x^2} + L_1 \right) \right. \\
&\quad \left. - e^{-\sqrt{r_a^2+x^2}/L_1} \left(\sqrt{r_a^2+x^2} + L_1 \right) \right]. \tag{S8}
\end{aligned}$$

Similarly, we compute the net force on the CS due to the constant CS-KT attraction as follows. KTs are uniformly arranged in a circle of radius R (Table S1), we can define the density of KTs $\rho_{KT} = N_{ch}/\pi R^2$. Then:

$$\begin{aligned}
\vec{f}_{CS-KT}^{attr}(x) &= \rho_{KT}R \int_0^{2\pi} d\theta f_{CS-KT}^{(0)} \cos \theta' \\
&= 2\pi\rho_{KT}f_{CS-KT}^{(0)} \frac{xR}{\sqrt{(R^2+x^2)}}. \tag{S9}
\end{aligned}$$

The energy of bringing a CS under the influence of this force field from ∞ to x is:

$$\begin{aligned}
E_{CS-KT}^{attr}(x) &= - \int_{\infty}^x 2\pi\rho_{KT}f_{CS-KT}^{(0)}R \frac{xdx}{\sqrt{R^2+x^2}} \\
&= - \int_{x_d}^x 2\pi\rho_{KT}f_{CS-KT}^{(0)}R \frac{xdx}{\sqrt{R^2+x^2}} \\
&= -N_{ch}f_{CS-KT}^{(0)} \left(\sqrt{R^2+x^2} - \sqrt{R^2+x_d^2} \right). \tag{S10}
\end{aligned}$$

Here we assume that the CS-KT attraction is constant for $x \leq x_d$ (Table S1), elsewhere it vanishes.

If a CS is fixed at x' and another CS is placed at x , the inter-CS attraction can be written as:

$$f_{CS-CS}(|x-x'|) = -f_{CS-CS}^{(0)}e^{-|x-x'|/L_1}. \tag{S11}$$

The energy of bringing one CS to x from ∞ in the presence of another CS fixed at x' is therefore:

$$\begin{aligned}
E_{CS-CS}(|x-x'|) &= f_{CS-CS}^{(0)} \int_{\infty}^{|x-x'|} e^{-|x-x'|/L_1} d|x-x'| \\
&= -f_{CS-CS}^{(0)}L_1 e^{-|x-x'|/L_1}. \tag{S12}
\end{aligned}$$

The total energy $E_{tot}(x)$ is obtained by summing the energies of CS-chromosome arm repulsion, CS-KT attraction and inter-CS attraction, respectively:

$$E_{tot}(x) = E_{CS-CH}^{rep}(x) + E_{CS-KT}^{attr}(x) + E_{CS-CS}(|x-x'|). \tag{S13}$$

We plot the total energy $E_{tot}(x)$ as a function of x , the axial distance between the CS and the center of the circular chromosomal ring (Fig. 5G, Fig. S4H).

SUPPORTING FIGURES

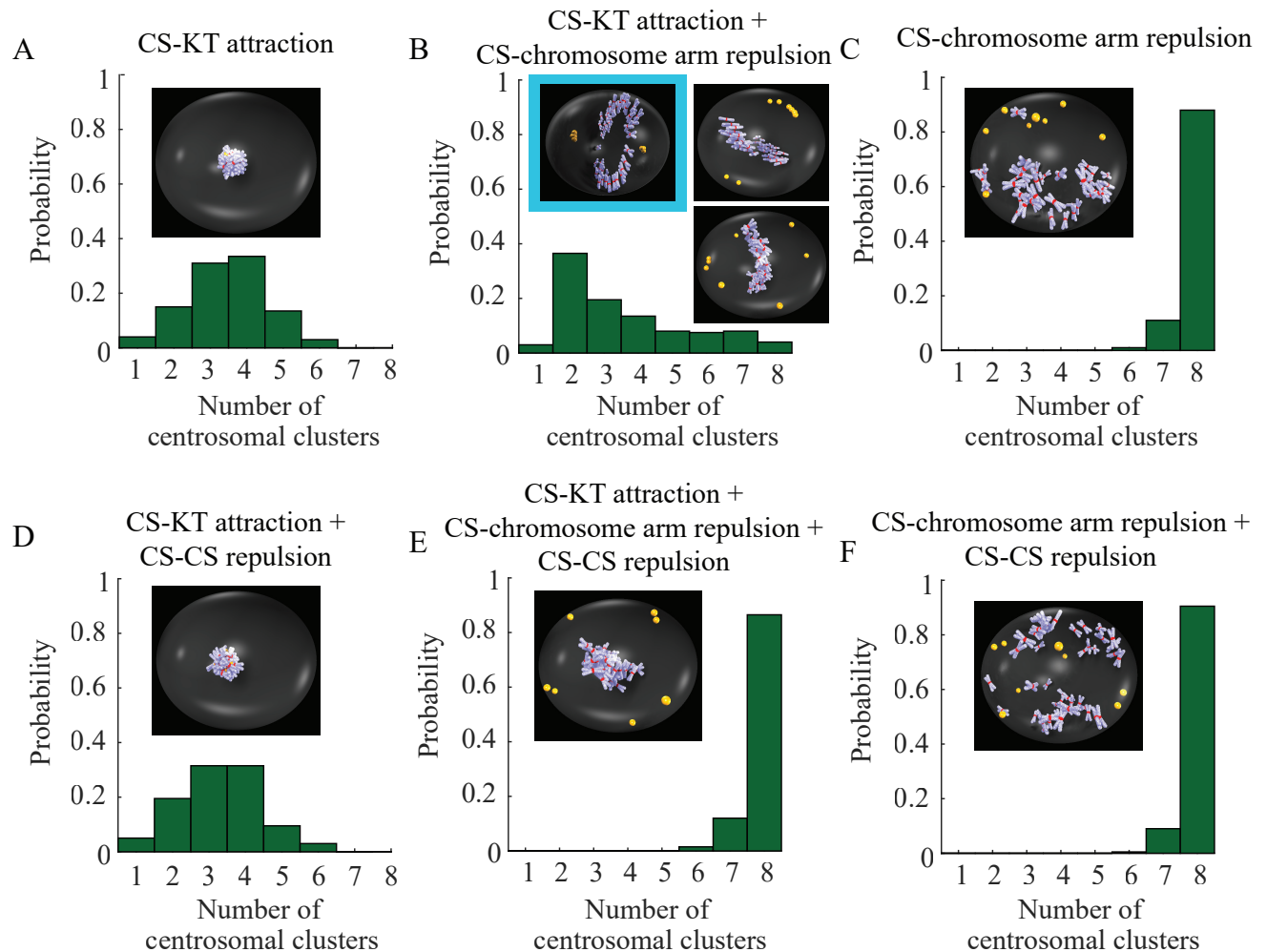


FIGURE S1 Spindle assembly in the cellular confinement in the absence of the CS-cortex attraction and without CS-CS attraction. CSs are yellow; chromosome arms are blue-and-white; KTs are red. Representative simulation snapshots for bipolar configurations in the inset are bordered in cyan frame. (A) Collapsed spindle in the presence of the CS-KT attraction and the absence of the inter-CS interaction. (B) Non-robust emergence of the bipolar spindle in the presence of the CS-KT attraction, CS-chromosome arm repulsion, and the absence of the inter-CS interaction. (C) Multipolar spindles develop under the sole influence of CS-chromosome arm repulsion. (D) Collapsed spindle when the CS-KT attraction is supplemented by the inter-CS repulsion. (E) Multipolar spindles develop when the CS-KT attraction and CS-chromosome arm repulsion are supplemented by the inter-CS repulsion. (F) Multipolar spindles develop when the CS-chromosome arm repulsion is combined with inter-CS repulsion.

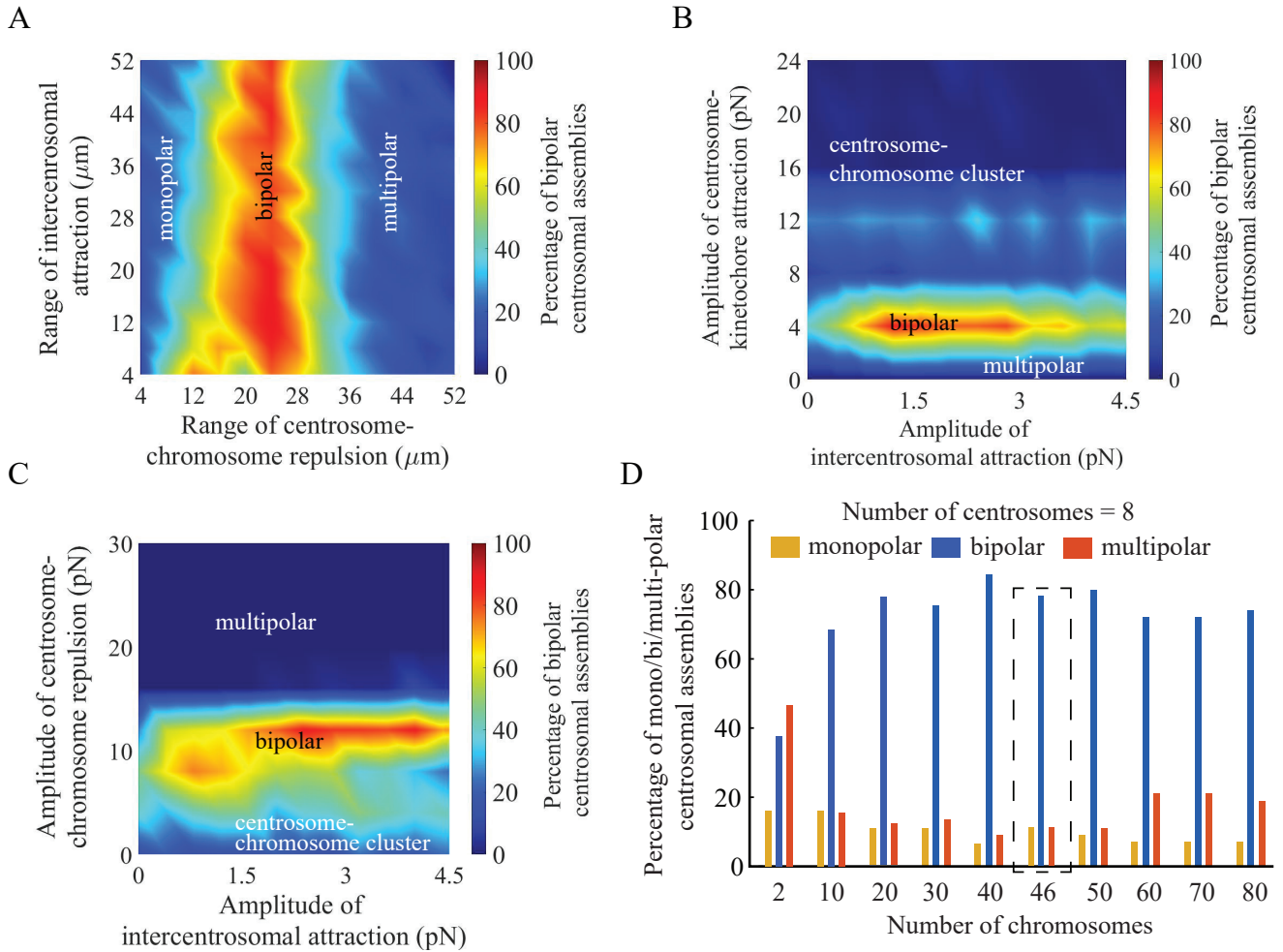


FIGURE S2 Model sensitivity to the parameters. (A) The bipolarity is sensitive to variations of the range of CS-chromosome arm repulsion and insensitive to that of the CS-CS attraction. (B) The bipolarity is sensitive to the amplitude of the CS-KT attraction but insensitive to that of the CS-CS attraction. (C) The bipolarity is sensitive to the amplitude of the CS-chromosome arm repulsion but insensitive to that of the CS-CS attraction. (D) Percentage of mono/bi/multi-polar spindles depending on the number of chromosomes. The statistics for 46 chromosomes (enclosed by dashed rectangle) represents the case of Fig. 4E.

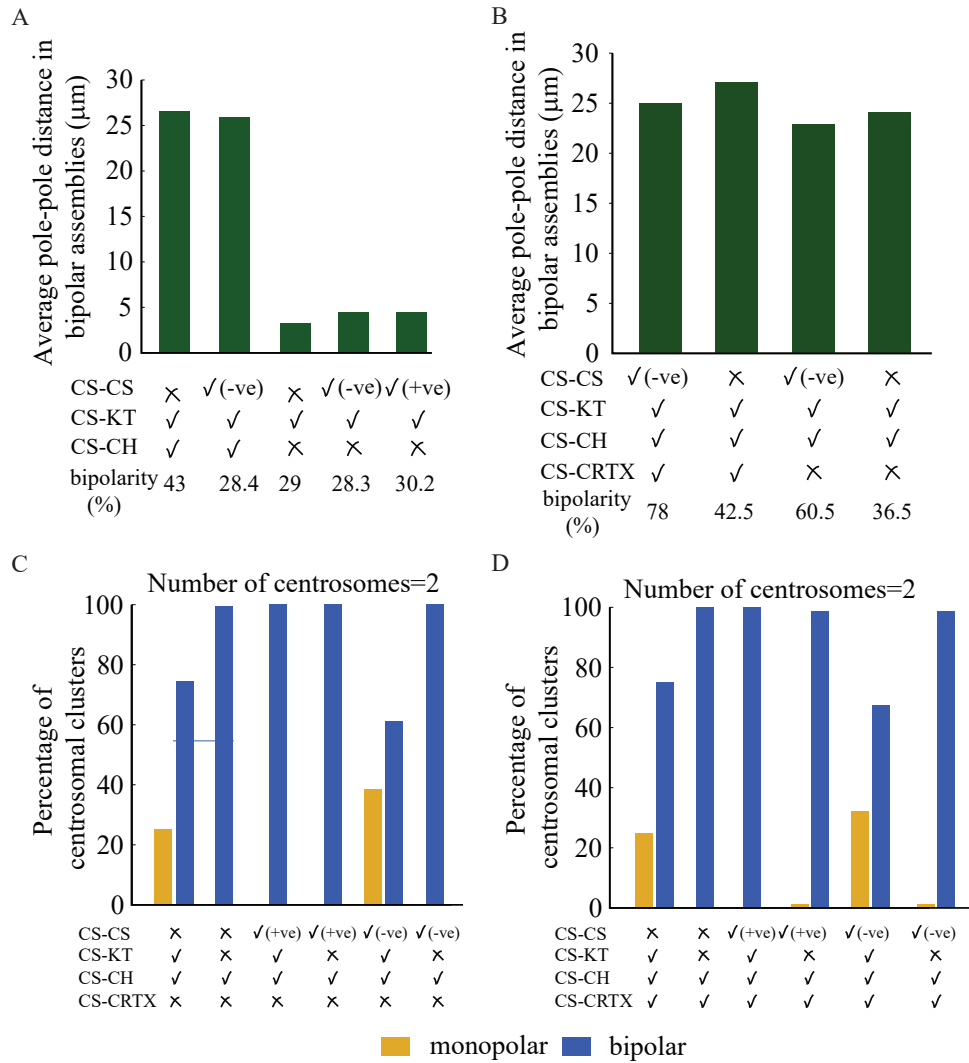


FIGURE S3 Dependence of the spindle characteristics on the force combinations. (A) Average pole-pole distance between two CS clusters in the bipolar spindles assembling under the influence of various force balances in unconfined geometry. ✓(✗) indicates presence (absence) of a particular interaction. -ve (+ve) denotes attractive(repulsive) forces. (B) between two CS clusters in the bipolar spindles assembling under the influence of various force balances in confined geometry. (C-D) The statistics of the mono/bi-polar spindles for various combinations of forces in confined geometry in the absence (C) or presence (D) of the centrosome-cortex attraction.

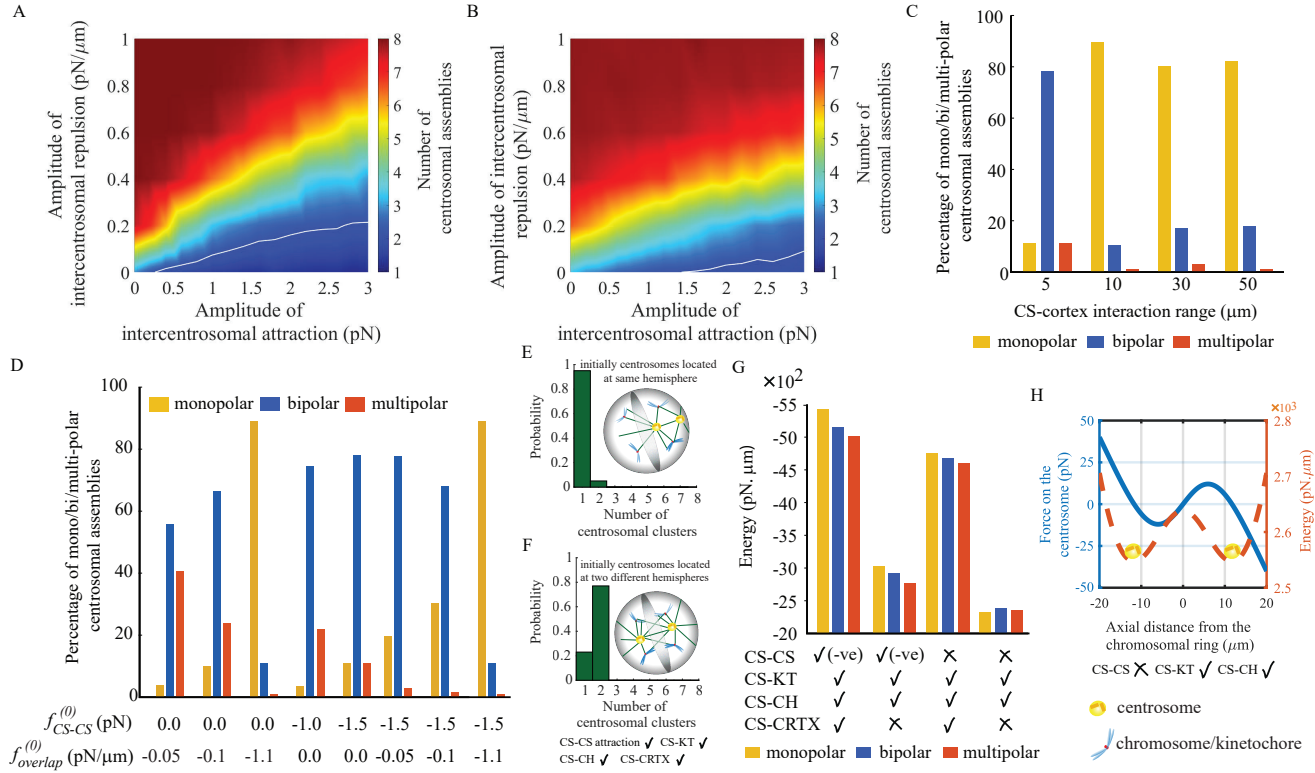


FIGURE S4 Additional spindle characteristics. (A-B) Bipolar centrosomal assembly contour (white solid line) shows the optimized balance of the inter-CS repulsion and attraction in unconfined (A) and confined (B) geometry. (C) Percentage of mono/bi/multi-polar spindles depending on the interaction range L_2 . (D) Percentage of mono/bi/multi-polar spindles depending on relative strengths of 'end-on' (f_{CS-CS} , dynein) and 'overlap' ($f_{overlap}$, kinesin-14) attractive inter-CS forces. (E-F) Percentage of mono/bi-polar spindles in 2-CS cells depending on whether two CSs are initially localized in the same (E) or different (F) hemispheres. The shaded equatorial plane distinguishes the hemispheres as shown in the inset. (G) Average spindle energies depending on the combinations of various forces in cellular confinement. (H) Dependence of the force and energy on the CS-CS distance in the thought experiment corresponding to Fig. 5G balance landscape in the absence of the inter-CS attraction.

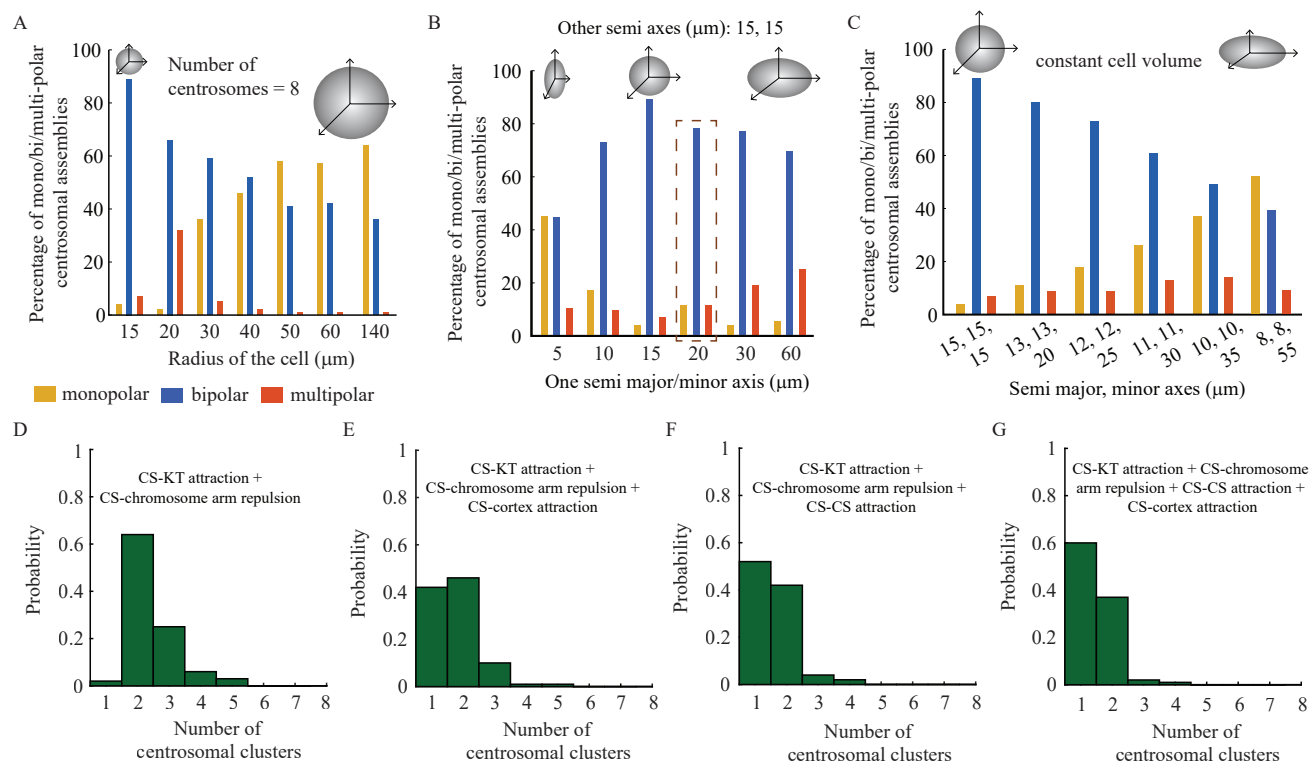


FIGURE S5 Percentages of mono/bi/multi-polar spindles depending on cellular geometry. Bipolarity is sensitive to cell size and shape. (A) Percentage of mono/bi/multi-polar spindles depending on the cell radius for spherical cells. Percentage of mono/bi/multi-polar spindle depending on the cell shape with the cell volume varied (B), with the cell volume roughly conserved (C). (D-G) Statistics of centrosomal assembly under various force combinations in flattened cells (cellular dimension: $5 \times 30 \times 30 \mu\text{m}^3$). Statistics in (G) corresponds to the forces of Fig. 4E in a flattened cell.

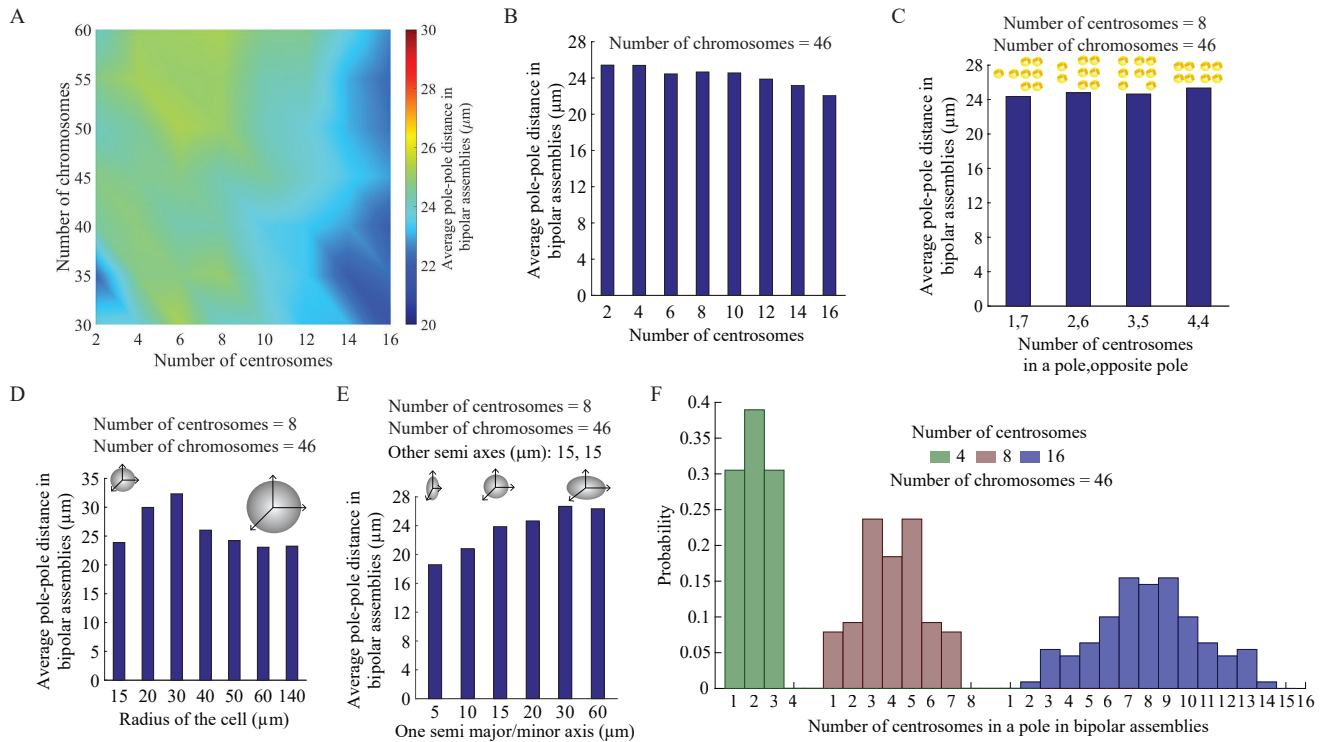


FIGURE S6 Additional features in bipolar spindles. (A) Average pole-pole distance between two CS clusters in the bipolar spindles is weakly sensitive to variations in the number of CSs and chromosomes. (B-C) Average pole-pole distance between two CS clusters in the bipolar spindles when the total number of CSs are varied (B), and kept fixed at 8 but segregated in clusters of different proportions between the poles (C). (D-E) Dependence of average pole-pole distance on cell radius (D), and cell shape (E). (F) Distributions of the number of CSs per cluster at the poles in the bipolar spindles.

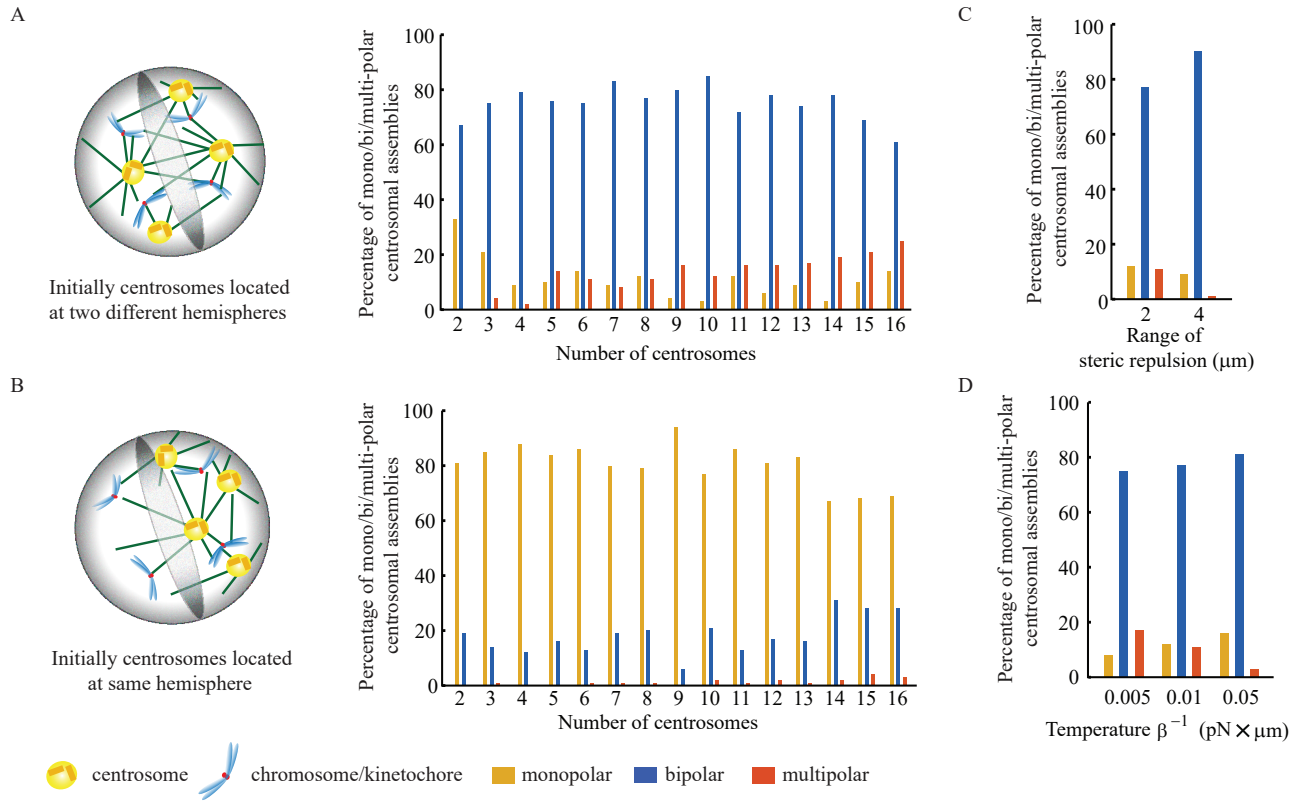


FIGURE S7 Spindle features depending upon the initial distribution of CSs and other parameters. (A-B) Percentages of mono/bi/multi-polar spindles depending on the CS number. CSs are initially localized in the different (A) and same (B) hemispheres, marked by the shaded equatorial plane. (C-D) Percentage of mono/bi/multi-polar spindles depending on the range of steric repulsion between pairs of chromosomes (C), on the inverse temperature β (D). Bipolarity does not alter much as the concerned parameters are varied.

SUPPORTING MOVIES

M1. Dynamic exploration of the energy space in the presence of intercentrosomal attraction, centrosome-kinetochore attraction and centrosome-chromosome arm repulsion in unconfined geometry results in the monopolar spindle. CSs are yellow; chromosome arms are blue-and-white; KTs are red.

M2. Dynamic exploration of the energy space in the presence of intercentrosomal repulsion, centrosome-kinetochore attraction, centrosome-chromosome arm repulsion and centrosome-cortex attraction results in the multipolar spindle. CSs are yellow; chromosome arms are blue-and-white; KTs are red.

M3. Dynamic exploration of the energy space in the presence of intercentrosomal attraction, centrosome-kinetochore attraction, centrosome-chromosome arm repulsion and centrosome-cortex attraction results in the bipolar spindle. CSs are yellow; chromosome arms are blue-and-white; KTs are red.

CODE

Numerical code is hosted at and can be downloaded from <https://github.com/sarkarapurba/MultiCentrosomalClustering.git>

Parameters	Description	Value	Notes & references
$f_{CS-CS}^{(0)}$	amplitude of intercentrosomal attraction (repulsion)	-1.5 (1.5) pN	Ratios of these forces, optimal for the bipolarity conditions, are found by numerical experiments. The absolute values of the force magnitudes do not, in fact, affect the predicted behavior. Nevertheless, the assumed dimensional values are consistent with the force of a few molecular motors per each interaction between any pair of bodies in the spindle. For details, see (1)
$f_{overlap}^{(0)}$	amplitude of intercentrosomal attraction (repulsion)	$\sim \pm 1$ pN/ μ m	
$f_{CS-KT}^{(0)}$	amplitude of centrosome-kinetochore attraction	-4.0 pN	
$f_{CS-CH}^{(0)}$	amplitude of centrosome-chromosome arm repulsion	10 pN	
$f_{CS-CRTX}^{(0)}$	amplitude of the centrosome-cortex attraction	-0.4 pN/ μ m ²	found by numerical experimentation; consistent with measurements in (2).
L_1	range of CS-CH and CS-CS interactions	20 μ m	found by numerical experimentation; The bipolarity is favored if this parameter is on the order of the cell radius.
L_2	range of CS-cortex interaction	5 μ m	found by numerical experimentation; The bipolarity is favored if this parameter is 3-6 times smaller than the cell radius.
L_{merge}	merging distance below which centrosomes are considered clustered	1.5 μ m	Order of magnitude of CS size (3)
β	inverse temperature	100 (pN \times μ m) ⁻¹	found by numerical experimentation; this parameter does not affect biology-relevant predictions.
additional parameters for analytical model			
r_a, r_b	inner and outer radius of the annular chromosome arrangement	12, 16 μ m	(4)
R	radius of the circular ring where kinetochores are arranged	14 μ m	
R_{cell}	radius of the cell	20 μ m	
x_d	cut off distance for kinetochore fiber attraction	20 μ m	

Table S1. List of model parameters

Geometry	Interactions				Polarity (%)			Remarks	
	<i>CS – CS</i>	<i>CS – KT</i> (-ve)	<i>CS – CH</i> (+ve)	<i>CS – CRTX</i> (-ve)	mono- polar	bi- polar	multi- polar		
Unconfined	\times	\checkmark	\times	\times	8	29*	63*	$(5, 6)^{a3}$	
	\times	\times	\checkmark	\times	0	0	100		
	\times	\checkmark	\checkmark	\times	7.2	43.3 [†]	49.5		
	\checkmark (-ve)	\checkmark	\times	\times	8.7	28.3*	63*		
	\checkmark (-ve)	\times	\checkmark	\times	1.8	5.5	92.7		
	\checkmark (-ve)	\checkmark	\checkmark	\times	70.3	28.4	1.4		$(6)^{a1}$
	\checkmark (+ve)	\checkmark	\times	\times	5.5	30.2*	64.3*		$\{ (7)^b \}$
	\checkmark (+ve)	\times	\checkmark	\times	0	0	100		
Confined (cortical pull absent)	\checkmark (+ve)	\checkmark	\checkmark	\times	0	0	100	$(6)^{a2}$	
	\times	\checkmark	\times	\times	4	15*	81*		
	\times	\times	\checkmark	\times	0	0	100	$(6)^{a3}$	
	\times	\checkmark	\checkmark	\times	3	36.5	60.5		
	\checkmark (-ve)	\checkmark	\times	\times	6	13*	61*		
	\checkmark (-ve)	\times	\checkmark	\times	0	0	100		
	\checkmark (-ve)	\checkmark	\checkmark	\times	26	60.5	13.5		
	\checkmark (+ve)	\checkmark	\times	\times	5	19.5*	75.5*		$\{ (7)^b \}$
\checkmark (+ve)	\times	\checkmark	\times	0	0	100			
\checkmark (+ve)	\checkmark	\checkmark	\times	0	0	100	$(6)^{a2}$		
Confined (cortical pull present)	\times	\checkmark	\times	\checkmark	2.5	17*	80.5*	$(8)^c$	
	\times	\times	\checkmark	\checkmark	0	0	100		
	\times	\checkmark	\checkmark	\checkmark	1	42.5	56.5		
	\checkmark (-ve)	\checkmark	\times	\checkmark	3	17.5*	79.5*		
	\checkmark (-ve)	\times	\checkmark	\checkmark	0	0	100		
	\checkmark (-ve)	\checkmark	\checkmark	\checkmark	11	78	11		
	\checkmark (+ve)	\checkmark	\times	\checkmark	2	20.5*	77.5*		$\{ (6, 9)^b \}$
	\checkmark (+ve)	\times	\checkmark	\checkmark	0	0	100		
\checkmark (+ve)	\checkmark	\checkmark	\checkmark	0	0	100			

TABLE S2 Statistics of the CS clusters. ‘-ve’ (‘+ve’) denotes attractive (repulsive) force fields. * Nearly collapsed CS-chromosome aggregate with 2 or more CS clusters. [†] A mixture of proper bipolar configurations with chromosomes at the midzone between two CS clusters and abnormal structures with 2 CS clusters. The values written in bold indicate significant number of bipolar clusters (> 35 %) among a mixed population of mono-/bi-/multi-polar centrosomal assemblies.

a. Kinesin-5 inhibition relates to monopolarity whereas dynein inhibition leads to unfocussed poles. Interestingly, double inhibition of dynein and kinesin-5 rescues bipolarity. In our model, kinesin-5 inhibition corresponds to the absence of CS-CS repulsion (*a1*) and dynein inhibition – to the absence of CS attraction to each other and cortex (*a2*). Hence, the double inhibition correlates with a force landscape having only two forces: CS-KT attraction and CS-chromosome arm repulsion (*a3*). Moreover, the over-expression of NuMA corresponds to the inhibition of CS-CS attraction promoting multipolarity. Mechanistically, this may also correlate with the presence of CS-CS repulsion and multipolarity (*a2*).

b. Plus end-directed Kinesin-5 activity on MTs plays a pivotal role in CS-CS repulsion. Experimentally it is observed that Kinesin-5 overexpression correlates with multipolar spindles. Our model also features multipolarity in the presence of CS-CS repulsion.

c. Loss of tension across K-fibres following the knockdown of proteins responsible for the CS-KT interaction leads to multipolarity.

Shapes of space in which chromosomes are packed in bipolar spindles								
Geometry	CS-CS attraction	CS-KT attraction	CS-CH repulsion	CS-CRTX attraction	Doughnut with a gap	Perfect doughnut	Sample size	
Unconfined	✗	✓	✓	✗	29	7	36	
Confined	✓	✓	✓	✓	44	18	62	
Confined	✓	✓	✓	✗	52	12	64	
Confined	✗	✓	✓	✓	26	14	40	
Confined	✗	✓	✓	✗	27	13	40	
Shapes of space in which chromosomes are packed in monopolar spindles								
Geometry	CS-CS attraction	CS-KT attraction	CS-CH repulsion	CS-CRTX attraction	Improper doughnut [†]	Random shape ^{**}	Sample size	
Unconfined	✗	✓	✓	✗	7	0	7	
Confined	✓	✓	✓	✓	22	0	22	
Confined	✓	✓	✓	✗	18	34	52	
Confined	✗	✓	✓	✓	2	0	2	
Confined	✗	✓	✓	✗	2	4	6	
Shapes of space in which chromosomes are packed in multipolar spindles								
Geometry	CS-CS attraction	CS-KT attraction	CS-CH repulsion	CS-CRTX attraction	Improper doughnut [†]	Single cluster	Multiple clusters ^{‡‡}	Sample size
Unconfined	✗	✓	✓	✗	26	2	4	32
Confined	✓	✓	✓	✓	4	0	11	15
Confined	✓	✓	✓	✗	12	2	9	23
Confined	✗	✓	✓	✓	28	3	15	46
Confined	✗	✓	✓	✗	32	2	9	43

Table S3. Classification of the shapes in which chromosomes are packed in bi/mono/multi-polar spindles. [†] Sparsely distributed chromosomes compared to the doughnuts in bipolar scenario. ^{**} Randomly distributed chromosomes, being roughly equidistant from the monopolar CS cluster. ^{‡‡} Often two large clusters with few stray chromosomes dispersed around.

SUPPORTING REFERENCES

1. Wollman, R., G. Civelekoglu-Scholey, J. M. Scholey, and A. Mogilner, 2008. Reverse engineering of force integration during mitosis in the *Drosophila* embryo. *Mol Syst Biol* 4:195.
2. Grill, S. W., J. Howard, E. Schäffer, E. H. K. Stelzer, and A. A. Hyman, 2003. The Distribution of Active Force Generators Controls Mitotic Spindle Position. *Science* 301(5632):518–21.
3. Loncarek, J., and M. Bettencourt-Dias, 2017. Building the right centriole for each cell type. *J Cell Biol* 217(3):823–835.
4. Magidson, V., C. B. O’Connell, J. Lončarek, R. Paul, A. Mogilner, and A. Khodjakov, 2011. The Spatial Arrangement of Chromosomes During Prometaphase Facilitates Spindle Assembly. *Cell* 146(4):555–567.
5. Brugués, J., V. Nuzzo, E. Mazur, and D. J. Needleman, 2012. Nucleation and Transport Organize Microtubules in Metaphase Spindles. *Cell* 149:554–564.
6. Oriola, D., D. J. Needleman, and J. Brugués, 2018. The Physics of the Metaphase Spindle. *Annual Review of Biophysics* 47:655–73.
7. Quintyne, N. J., J. E. Reing, D. R. Hoffelder, S. M. Gollin, and W. S. Saunders, 2005. Spindle multipolarity is prevented by centrosomal clustering. *Science* 307:127–129.
8. Maiato, H., and E. Logarinho, 2014. Mitotic spindle multipolarity without centrosome amplification. *Nature Cell Biology* 16(5):386–394.
9. Drosopoulos, K., C. Tang, W. C. Chao, and S. Linardopoulos, 2014. APC/C is an essential regulator of centrosome clustering. *Nat Commun* 5:3686.